haematologica
Journal of The Ferrata Storti Foundation

The architecture of neoplastic follicles in follicular lymphoma; analysis of the relationship between the tumor and follicular helper T-cells

by William Townsend, Marta Pasikowska, Deborah Yallop, Elizabeth H. Phillips, Piers E.M. Patten, Jonathan R. Salisbury, Robert Marcus, Andrea Pepper, and Stephen Devereux

Haematologica 2019 [Epub ahead of print]

Citation: William Townsend, Marta Pasikowska, Deborah Yallop, Elizabeth H. Phillips, Piers E.M. Patten, Jonathan R. Salisbury, Robert Marcus, Andrea Pepper, and Stephen Devereux. The architecture of neoplastic follicles in follicular lymphoma; analysis of the relationship between the tumor and follicular helper T-cells.
Haematologica. 2019; 104:xxx
doi:10.3324/haematol.2019.220160

Title

The architecture of neoplastic follicles in follicular lymphoma; analysis of the relationship between the tumor and follicular helper T-cells.

Short title

Follicular helper T-cells in FL

Authors

William Townsend,[1,2] Marta Pasikowska,[1] Deborah Yallop,[1,3] Elizabeth H. Phillips,[1] Piers E.M. Patten,[1,3] Jonathan R. Salisbury,[4] Robert Marcus,[3] Andrea Pepper,[5]* and Stephen Devereux.[1,3]*

* AP and SD contributed equally to this study.

Affiliations

[1]Department of Haematological Medicine, Rayne Institute, King's College London, London, UK

[2]Department of Haematology, University College London Hospitals NHS Foundation Trust, London, UK

[3]Department of Haematology, King's College Hospital, London, UK

[4]Department of Histopathology, King's College Hospital, London, UK

[5]Department of Clinical and Experimental Medicine, Brighton and Sussex Medical School, Brighton, UK

Corresponding Author:

Name: Dr William Townsend

Address: Department of Haematology, University College London Hospitals NHS Foundation Trust, London, NW1 2BU. UK

Email: william.townsend@nhs.net

Phone: +447747030265

Disclosures:

SD discloses consultancy fees and honoraria from Gilead.

WT discloses consultancy fees and honoraria from Roche and Gilead.

RM discloses consultancy fees and honoraria from Roche.

Abstract

CD4+ T-follicular helper cells are essential for the survival, proliferation, and differentiation of germinal center B-cells and have been implicated in the pathogenesis of follicular lymphoma. To further define the role of these cells in follicular lymphoma, we used multiparameter confocal microscopy to compare the architecture of normal and neoplastic follicles and next generation sequencing to analyze the T-cell receptor repertoire in follicular lymphoma lymph nodes. Multiparameter analysis of lymph nodes showed that the proportion of T-follicular helper cells in normal and neoplastic follicles is the same and that the previously reported increase in T-follicular helper cell numbers in follicular lymphoma is thus due to an increase in the number and not content of follicles. As in normal germinal centers, T-follicular helper cells were shown to have a close spatial correlation with proliferating B-cells in neoplastic follicles, where features of immunological synapse formation were observed. The number of T-follicular helper cells in follicular lymphoma correlate with the rate of B-cell proliferation and T-follicular helper cells co-localized to Activation Induced Cytidine Deaminase expressing proliferating B-cells. T-cell receptor repertoire analysis of follicular lymphoma lymph nodes revealed that follicular areas are significantly more clonal when compared to the rest of the lymph node. These novel findings show that neoplastic follicles and germinal centers share important structural features and provide further evidence that T-follicular helper cells may play a role in driving B-cell proliferation and genomic evolution in follicular lymphoma. Our results also suggest that targeting this interaction would be an attractive therapeutic option.

Introduction

Follicular lymphoma (FL) is a neoplasm of germinal center B-cells that is usually characterized by the t(14;18) translocation and over-expression of BCL2.(1, 2) The clinical course is variable, prognosis is difficult to predict, and it is typically incurable.(3, 4) The tumor is infiltrated by numerous subsets of non-malignant T-cells(5-8). Gene expression profiling (GEP) studies have shown that prognosis in FL can be correlated with the signature of non-malignant T-cells of the microenvironment rather than the tumor itself, indicating that the microenvironment is important in the pathogenesis of this disease.(9, 10) The relationship between FL B-cells and their microenvironment is complex; non-malignant T-cells may either promote or inhibit tumor growth whilst the tumor itself can influence the composition of the microenvironment.(11, 12) Many groups have investigated the impact of microenvironment-related factors on outcome.(10, 13-16) These studies have, however, yielded contradictory results, most likely because of differences in patient populations studied, therapy administered and technical limitations of single parameter immunohistochemistry (IHC) that preclude accurate identification of cell subsets.

In normal germinal centers (GCs), B-cells are critically dependent on interactions with $CD4^{pos}$ follicular helper T-cells (T_{FH}) (17-20), which are characterized by expression of PD-1, ICOS, CXCR5, CXCL13, IL-21 and IL-4 and the transcription factor BCL6 (19, 21, 22). T_{FH} provide signals necessary for the survival and proliferation of GC B-cells and induce expression of activation induced cytidine deaminase (AID), a DNA modifying enzyme that initiates somatic hypermutation (SHM) and class switch recombination (CSR) leading to a class-switched, high-affinity antibody response.(17, 19, 20, 23)

FL follicles and normal GCs share a number of features; FL B-cells have a similar phenotype and GEP as their normal counterparts and neoplastic follicles contain both follicular dendritic cells (FDCs) and T-cells. Studies performed on disaggregated FL LNs have previously demonstrated an enrichment of IL-4-producing T_{FH} in FL with a distinct gene expression profile and the ability to support FL B-cell growth and modify stromal cell function in-vitro.(24-28) The anatomic relationship between T_{FH} and FL B-cells and how closely this mimics the situation in normal GCs has, however, not previously been studied.

In this study we compared the architecture of normal GCs and neoplastic follicles, specifically focusing on the spatial relationship between B-cells and T_{FH} using multiparameter confocal immunofluorescence microscopy and semi-automated image analysis. We found that T_{FH} - as identified by surface expression of CD4, PD1, and ICOS - constitute a similar proportion of $CD4^{pos}$ T-cells in FL as they do in normal GCs. They colocalize and form synapses with proliferating neoplastic B-cells, which also express the DNA modifying enzyme AID. Finally, TCR repertoire analysis revealed that T-cells in neoplastic follicles are significantly more clonal than those in interfollicular areas, suggesting a role for antigen stimulation in this process. Overall, our findings further highlight the role of the microenvironment in FL and are relevant to the mode of action of new therapies such as those targeting antigen receptor signaling and the PD1/PDL1 axis.(29-32)

Methods

Patient samples

Formalin fixed paraffin embedded (FFPE) LN biopsies were obtained from 25 patients with histologically confirmed untreated or relapsed FL including 3 cases of Grade 3b FL, and 8

patients with reactive lymphadenopathy. Patients with relapsed FL had not received any treatment for at least 12 months. Clinical details are presented in Supplementary Tables 1 and 2. Ethical approval was obtained from the UK national research ethics committee, reference 13/NW/0040.

Immunofluorescent confocal microscopy

FFPE LN sample preparation steps including deparaffinization, antigen retrieval, and staining are described in the supplemental methods. All images were acquired on a Nikon Eclipse Ti-E microscope and analyzed using Nikon elements NIS Advanced Research software. Full descriptions of imaging and analysis techniques including the use of binary layers for image analysis are presented in the supplemental methods and further explained in Figure S1.

Laser micro-dissection, DNA extraction, and TCR sequencing

Follicles were highlighted by conventional IHC staining for BCL6. Follicular and interfollicular areas were dissected from sequential 10μm FL sections using a laser capture microscope (PALM, Carl Zeiss MicroImaging, Jena, Germany). After DNA extraction, TCRβ sequences were subject to multiplex PCR amplification prior to next generation sequencing (Adaptive Biotechnologies, Seattle, WA. USA) (33). TCRVβ CDR3 regions and their component V, D and J segments were identified using the IMGT definitions.(34) Sequences not corresponding to a CDR3 were discarded and unique clones defined by the presence of more than one identical productive CDR3 DNA sequence. The number and size of each clone was determined and the richness, clonality and overlap of the follicular and interfollicular TCR repertoires determined (see supplementary methods).

Statistical analysis

Statistical analysis was performed using GraphPad Prism software v5 (GraphPad Software Inc, La Jolla, California, USA). Normally distributed values are presented as the mean (+/- standard deviation), non-normally distributed values are presented as median (+/- interquartile range). Further details of statistical analysis are presented in the supplementary methods.

Results

Normal and neoplastic follicles contain similar numbers of T follicular helper cells.

$CD4^{pos}$ T-cells were predominantly located in the interfollicular areas of reactive and FL LNs but discrete populations were also present within the GCs and malignant follicles. We investigated the phenotype of these by staining for CD4, PD-1 and ICOS simultaneously. Within GCs of reactive LNs 33.05% (24.7-43.7) of $CD4^{pos}$ T-cells co-expressed PD-1 and ICOS (T_{FH} phenotype) and these were distributed predominantly in the light zones (Figure 1a). In FL, 25.0% (18.5-28.7) of follicular $CD4^{pos}$ T-cells expressed both PD-1 and ICOS and were located at the follicular border or diffusely distributed within the follicles (Figure 1b). The proportion of $CD4^{pos}$ cells co-expressing PD-1 and ICOS was not significantly different between FL follicles and GCs (Figure 1c). $CD4^{pos}PD\text{-}1^{pos}ICOS^{pos}$ cells were tightly restricted to the GCs of reactive LNs and FL follicles with only 0.34% (0.26-1.13) and 3.63% (1.89-6.15) of non-GC or interfollicular FL $CD4^{pos}$ cells co-expressing PD-1 and ICOS respectively.

In FL, although 46.9% (34.7-51.9) of follicular $CD4^{pos}$ cells expressed PD-1, only about 50% of these co-expressed ICOS indicating that there are at least 2 distinct populations of $CD4^{pos}PD\text{-}1^{pos}$ cells within FL follicles, highlighting the importance of using all three

parameters for identification of T_{FH} cells. There was no difference in the proportion of $CD4^{pos}$ cells that co-expressed PD-1 and ICOS by histological grade in FL (Figure S8), however, as the number and size of neoplastic follicles increase with histological grade, so must the absolute number of T_{FH}.

To investigate differences in T-cells located in the follicles and interfollicular areas of FL, the intensity of CD4 and PD-1 expression were measured. CD4 expression was 30.7% lower in follicular $CD4^{pos}$ T-cells than in their interfollicular counterparts suggesting that these represent a distinct population of T-cells (Figure S2). Whilst $CD4^{pos}PD\text{-}1^{pos}ICOS^{pos}$ cells were restricted to the follicles, $CD4^{pos}PD\text{-}1^{pos}ICOS^{neg}$ cells were present in the interfollicular area where 9.3% (5.1-26.4) of $CD4^{pos}$ cells expressed PD-1. The intensity of PD-1 expression was significantly higher in follicular $PD\text{-}1^{pos}$ T-cells than interfollicular $PD\text{-}1^{pos}$ T-cells (Figure S2) consistent with them being T_{FH}.(35) Additional co-staining experiments demonstrated that these cells had a composite $CD3^{pos}$,$CD8^{neg}$,$PD\text{-}1^{pos}$,$ICOS^{pos}$,$BCL6^{pos}$, $CXCR5^{pos}$, $TBET^{neg}$ phenotype further confirming their identity as T_{FH} (Figure 1d, and S2c). Although CXCR5 has frequently been used to identify T_{FH} by flow cytometry, we found that it was unhelpful in identifying this cellular subset by microscopy since most T-cells present within these structures were $CXCR5^{pos}$ and it therefore did not help to distinguish them from other GC/follicularly located cells (Figure S2c). It was not possible to use CD4 in these experiments as the antibody is the same species as the BCL6. No $BCL6^{pos}$ cells were found to be $CD8^{pos}$ therefore the substitution for CD3 was acceptable (Figure S2d). The intensity of BCL6 staining in T_{FH} was lower than that observed in FL B-cells but higher than in other T-cells (Figure S2b). Although 25.0% (6.0-28.0) of $ICOS^{pos}$ T-cells and 4.0% (1.0-8.0) of $PD\text{-}1^{pos}$ T-cells within FL follicles were $FOXP3^{pos}$, only a minority of dual $PD\text{-}1^{pos}ICOS^{pos}$ T-cells expressed

FOXP3, (Figure S3). In comparison to FL, very few FOXP3^{pos} T-cells were identified within the GCs of reactive LNs where they were exclusively located outside the GCs (Figure S3b).

These findings confirm that the majority of GC or follicular CD4^{pos} cells that strongly express PD-1 and ICOS are T_{FH} and constitute the same proportion of CD4+ cells in normal and neoplastic follicles.

T_{FH} co-localize with proliferating B-cells

Next, we investigated if there is a spatial relationship between proliferating B-cells and T_{FH} in reactive and neoplastic follicles. An ideal panel of CD20, Ki67, CD4, PD-1 and ICOS was not possible for technical reasons. However, co-staining for CD20, Ki67, and CD3 (Figure S4) showed that in both normal GCs and neoplastic follicles the majority of Ki67^{pos} cells are CD20^{pos} B-cells. Also, as most PD-1^{Hi} cells were ICOS^{pos} , it enabled T_{FH} cells to be identified using just two parameters; CD4 and high PD1 expression.

In normal GCs a close spatial correlation between Ki67^{pos} cells and CD4^{pos}PD-1^{Hi} cells was evident in the light zone of all cases (Figure 2a). Automated image analysis showed that 63.1% ±15.9 of Ki67^{pos} cells in the light zones were in direct contact with CD4^{pos}PD-1^{Hi} cells, furthermore, the high density of T_{FH} in this compartment meant that the majority of Ki67^{pos} B-cells were in close proximity to ≥1 T_{FH}. The majority of these PD-1^{Hi} cells were also ICOS^{pos} with 53.9% ±14.2 of Ki67^{pos} cells in contact with PD-1^{pos}ICOS^{pos} cells. In GC light zones, Ki67^{pos} B-cells were significantly more likely than Ki67^{neg} B-cells to be in contact with T_{FH} in all cases studied (P<0.005 in each GC examined) (Figure 2c).

In the highly proliferative dark zones, there were few T_{FH} and a very high number of Ki67^{pos} B-cells. The closely packed Ki67^{pos} B-cells could not be separated by automated image

analysis and therefore accurate calculation of the proportion of $Ki67^{pos}$ cells in contact with T_{FH} could not be performed in the dark zones. It is clear from visual inspection, however, that the degree of spatial correlation between these cells is much lower in the dark zones than in the light zones (Figure 2b).

A close spatial relationship between $Ki67^{pos}$ B-cells and $CD4^{pos}PD\text{-}1^{Hi}$ T-cells was also found in FL and, in contrast to normal GCs, all areas with high Ki67 also had increased numbers of T_{FH} cells. In FL 41.0% ±13.6 of $CD20^{pos}Ki67^{pos}$ cells were found to be in direct contact with $CD4^{pos}PD\text{-}1^{Hi}$ cells, although the level of co-localization was significantly lower than in GCs ($p=0.003$), there was a high level of co-localization in both settings (Figure 3a). High power images and 3D Z-stack reconstructions revealed that there was very close contact between these cells, and $Ki67^{pos}$ cells were frequently observed to be in contact with more than one $CD4^{pos}PD\text{-}1^{Hi}$ cell simultaneously. Staining for Ki67, PD-1, and ICOS revealed that 84.7% ±11.1 of the $PD\text{-}1^{Hi}CD4^{pos}$ cells in contact with $Ki67^{pos}$ cells were also $ICOS^{pos}$ and therefore likely to be T_{FH} (Figure 3b).

$Ki67^{pos}CD20^{pos}$ FL B-cells were significantly more likely than $Ki67^{neg}CD20^{pos}$ FL B-cells to be in direct contact with T_{FH} in each case examined, ($P<0.0001$ for each specimen) (Figure 3c).

Relationship between Ki67, T_{FH} cells and histological grade

The area of the Ki67 binary layer and the corresponding number of $Ki67^{pos}$ cells counted by automated analysis increased with histological grade (Figure 4a). The area of the $PD\text{-}1^{pos}ICOS^{pos}$ intersection was closely correlated with the number of $Ki67^{pos}$ cells and histological grade demonstrating that, in higher grade cases with a higher proliferation rate, the absolute number of T_{FH} is increased (Figure 4b). The degree of colocalization between Ki67+ B-cells and T_{FH} was, however, similar across all histological grades. Thus, in cases with

low Ki67 there were few T_{FH} and in cases with high Ki67 there were more T_{FH}, but the extent of co-localization remained relatively constant (Figure 4c). There was also a correlation between the number of $Ki67^{pos}$ cells and the number of T_{FH} in normal GCs (r = 0.55, P = 0.019, n=17 GCs from n=4 samples, Figure S7).

Proliferating cells in contact with T_{FH} express AID

Since T_{FH} have been implicated in initiating SHM and CSR through induction of AID in GCs,(20) we investigated if there was a spatial relationship between T_{FH} and AID^{pos} cells. AID was restricted to $Ki67^{pos}$ cells in FL, 63% ±8.8 of which were AID^{pos} and 39.8% ±9.7 of $AID^{pos}Ki67^{pos}$ cells were in direct contact with $PD\text{-}1^{Hi}$ cells. As we had established that most $PD\text{-}1^{Hi}$ cells in contact with $Ki67^{pos}$ cells were $ICOS^{pos}$, we can predict that the majority of $PD\text{-}1^{Hi}$ cells in contact with $AID^{pos}Ki67^{pos}$ cells were T_{FH} (Figure S5). AID was similarly restricted to $Ki67^{pos}$ cells of GCs where close association with $PD\text{-}1^{Hi}$ cells was evident in the light zones (Figure S5c).

PD-L1

PD-L1 has previously been reported to be absent from the surface of FL B-cells(36) and we found no evidence that PD-L1 was strongly expressed on the $Ki67^{pos}$ cells in contact with $PD\text{-}1^{Hi}$ cells. Instead, PD-L1 was expressed mainly on interfollicular $CD23^{neg}$ cells (Figure S6). The identity of these cells was not further investigated in this study.

Features of synapse formation

The close spatial relationship between $Ki67^{pos}$ FL B-cells and T_{FH} was further investigated in high power images where morphological features indicating the formation of immunological synapses were identified. Features included: T_{FH} cell membrane projections encompassing the $Ki67^{pos}$ cells, overlapping of the B and T-cell membranes, distortion of T-cell nuclei away

from points of cell contact and significantly increased intensity of CD4, PD-1, and ICOS expression at points of cell contact (Figure 5)(37). The intensity of expression of CD4, PD-1, and ICOS at points where T_{FH} were in contact with $Ki67^{pos}$ cells was formally quantified by defining the perimeter of the T-cell membrane and measuring the intensity of fluorescence at each pixel around the perimeter. The area under the curve for intensity at the point of cell contact was compared with an equivalent length of cell membrane at the opposite pole (Figure 5b). Similar features indicating synapse formation were identified in GC light zones but the high number of closely-packed $Ki67^{pos}$ cells and T_{FH} in GCs precluded the same analytic method being used because T_{FH} in GCs were usually in contact with more than one $Ki67^{pos}$ cell simultaneously.

TCR repertoire within follicles shows evidence of antigen restriction

In view of the close spatial relationship observed between T-cells and proliferating tumor cells, we investigated whether T-cells within the follicles show evidence of antigen restriction by performing TCR Vβ NGS of genomic DNA from laser dissected follicular and interfollicular areas from 5 FL samples. The degree of restriction of the TCR Vβ repertoires in FL neoplastic follicles and interfollicular areas was assessed in several ways. First, we estimated the richness of the repertoire in each compartment by determining the number of different clones present per ng of input DNA which, since we were analysing genomic DNA, was proportionate to the total cell number. The interfollicular areas contained more T-cell clones per ng of input DNA than the intrafollicular regions, however, this did not quite reach statistical significance (p=0.06, Table S4). We also calculated the clonality index(38) (see supplementary methods for further details). In each of 5 cases examined, the clonality of the follicular T-cells was greater than in the interfollicular areas (*P*=0.0317, Figure 6a).

We also calculated the proportion of the TCR repertoire in each compartment that was accounted for by high frequency clones.(39) Compared to the interfollicular areas, the follicular regions were dominated by high frequency clones (figure 6b). For example, the top 50 most frequent clones made up a mean of 19% of all clones in the follicular areas (95% CI 17-21) compared to 9.8% in the interfollicular region (95% CI 6.1-13.4) p=0.0002, n=5.

As expected from their different phenotypes, the clones present in the follicular and interfollicular areas of the same sample were markedly different, indicating that the TCR repertoires of the follicular and interfollicular areas are distinct (Figure 6c).

Discussion

In this study we compared the structure of neoplastic follicles in FL with GCs in reactive LNs, focusing on T_{FH}, their relationship with proliferating B-cells and TCR repertoire. Although T_{FH} have previously been reported to be present in the FL microenvironment (24-27), these studies were performed on disaggregated LNs and this is the first time that their spatial organization has been investigated in-situ in this way. Using multi-parameter immunofluorescent confocal microscopy, we demonstrated that T_{FH} – as identified by surface expression of CD4, PD1, and ICOS - constitute a similar proportion of $CD4^{pos}$ T-cells in FL as in reactive LNs and form synapses with proliferating $Ki67^{pos}$ tumor cells which express the DNA modifying enzyme AID. The number of T_{FH} in neoplastic follicles correlates with the level of tumor proliferation and histological grade, and there is evidence for antigen restriction, as supported by the more clonal TCR repertoire found within neoplastic follicles compared to interfollicular areas.

These findings are novel and of significance for a number of reasons. First, in contrast to previous work on disaggregated FL LNs, which showed an increase in the total number of T_{FH}(24, 25, 40), we found that FL follicles contain T_{FH} in similar proportions to normal reactive GCs. This discrepancy likely relates to the fact that in FL, LN architecture is usually effaced by many closely packed follicles, whereas in normal tissues the interfollicular areas, which contain many fewer T_{FH}, are more extensive. Thus, although the overall T_{FH} content of FL LNs is increased compared to normal (25), this is because of the larger number of follicles in the tumor and when neoplastic and normal follicles are compared directly, the numbers are the same. This finding underlines the need to complement data obtained from disaggregated tissues with anatomic studies.

Our use of multiparameter microscopy permitted the spatial relationship between T_{FH} and B-cells to be closely investigated and this also provided new insights. T_{FH} are essential for providing normal GC B-cells with signals necessary for their survival, proliferation and maturation.(19, 41) To our knowledge, this is the first time that the intimate relationship between $Ki67^{pos}$ B-cells and T_{FH} has been demonstrated *in-situ* in human LNs in this way and our observations are in keeping with the pivotal role they play in the normal GC reaction. Importantly, we also found that the close spatial association of $Ki67^{pos}$ B-cells and T_{FH} is recapitulated in FL, as 41% of $Ki67^{pos}$ FL B-cells were in direct contact with T_{FH} and were significantly more likely to be in direct contact with T_{FH} than non-proliferating cells. The observed close spatial correlation between the two cell types is thus not due to chance and suggests that T_{FH} are involved in functionally important interactions with the tumor. This corroborates and advances findings from previous *in-vitro* experiments which showed that FL T_{FH} provide signals for B-cell survival.(25, 27)

We also found a correlation between the numbers of T_{FH} and $Ki67^{pos}$ B-cells in both normal GCs and neoplastic follicles and that, in FL, the number of T_{FH} increase with histological grade. The relationship between number of T_{FH} and rate of B-cell proliferation observed in our study has not been reported previously in FL but is consistent with previous data showing that the regulation of GC size and B-cell number is critically dependent on the number of T_{FH} (17, 19, 23). This adds to the evidence that T_{FH} are central to the pathogenesis of FL, just as they are essential in the normal GC reaction. Furthermore, the degree of co-localization (the proportion of $Ki67^{pos}$ B-cells in contact with one or more T_{FH}) remained constant as histological grade increased, with no significant change in the proportion of $Ki67^{pos}$ cells in contact with T_{FH} in grade 3a or 3b disease compared to grade 1-2 disease, suggesting that interaction with T_{FH} remains important regardless of histological grade.

Our studies also underline the crucial importance of using a multi-parameter approach to define and quantify the complex T-cell subsets present in the FL microenvironment. No single antigen or transcription factor specifically identifies T_{FH} and this is the first study reporting the presence of T_{FH} in FL *in-situ* using techniques that overcome the limitations of traditional IHC. By using co-staining for ICOS and BCL6 we were able to show that only half of the PD1 expressing cells neoplastic follicles are T_{FH} . Single parameter analysis of PD1 would therefore lead to significant overestimate of T_{FH} numbers perhaps explaining, at least in part, why previous IHC studies have yielded divergent results with regards to the impact of different T-cell infiltrates on prognosis.(10, 13-16)

Previous in-vitro studies have shown that peripheral blood T-cells in FL are dysfunctional and form impaired synapses with B-cells.(40, 42) In the present study, however, we found features that suggest normal synapse formation between $Ki67^{pos}$ tumor cells and T_{FH} within

the LN.(43) This divergence from previous research may be because we examined the interactions between T_{FH} and $Ki67^{pos}$ cells *in-situ* in human tissue rather than in an ex-vivo system using peripheral blood derived cells. It also remains possible that there are other subsets of

non T_{FH} cells in the FL microenvironment that are dysfunctional and have an impaired ability to form immunological synapses.

In addition to promoting GC B-cell proliferation, interaction with T_{FH} cells also induces AID expression which induces somatic hypermutation and class switch recombination. Off-target action of AID has previously been proposed to lead to the accumulation of mutations required for germinal center-derived lymphomas to develop or progress and has been associated with transformation of FL.(44, 45) The close spatial association between T_{FH} and $AID^{pos}Ki67^{pos}$ FL B-cells observed in the present study is compatible with this theory.

Finally, NGS analysis of the TCR repertoire of follicular and interfollicular areas of FL LNs showed that the neoplastic follicles are significantly more clonal and dominated by high frequency clones compared to the interfollicular regions. As expected from their divergent phenotype, very little repertoire overlap between the two compartments was present. PCR-based analyses of TCR repertoire on small samples are known to suffer from a number of potential limitations including sampling effects and errors introduced during the amplification process, which may lead to apparent skewing.(46) Whilst we cannot completely exclude these possibilities, we minimized the risk by direct, intra-patient comparison in the same assay run, and, of note, our findings were consistent in all 5 cases studied. Another possibility is that the demonstrated differences in TCR repertoire relate to the greater number of T-cells found in the interfollicular regions compared to the follicles.

Whilst T-cell numbers undoubtedly do differ between these two areas, significant difference in the clonality index, which takes into account the number of unique clones present, were observed (figure 6a). Furthermore, the repertoire of the intrafollicular area was strikingly dominated by high frequency clones; for example, the top 50 clones accounted for a mean of 19%(CI 17-21%) of all clones present, compared to 9.7%(CI 6.1-13.4%) in the interfollicular areas (p=0.0002).

Taken together, these findings suggest that the interactions between B-cells and activated T_{FH} that induce B-cell proliferation and differentiation and lead to the generation of high affinity antibody in normal GCs may be recapitulated within the follicles of FL.(19, 41) Since T_{FH} may be involved in processes fundamental to disease progression, such as clonal expansion and genomic evolution of the tumor, our results suggest that they would be an attractive target for novel therapies. This is especially relevant in the era of drugs that target antigen receptor signaling such as PI3-kinase inhibitors, which affect both B- and T-cell receptor pathways. Our results are also relevant to understanding the mechanism of action of drugs that target PD-1 expressing cells, which have been shown to be effective in FL and other lymphomas.(29-31) It is clear that whilst some of the PD-1 expressing cells in the FL LNs are indeed T_{FH}, many are not and these may represent exhausted effector cells. Blockade of PD-1 in the latter case may unmask antitumor immunity and lead to disease regression. The impact of interrupting PD-1 function in T_{FH} is, however, less clear as the role of the PD-1 axis in T_{FH} function is not fully established. These findings add another level of complexity to our understanding of the FL tumor microenvironment and underline the necessity of using multi-dimensional methods in future studies.

Acknowledgements

This research was funded by grants from the British Society of Haematology in partnership with the Roger Counter Foundation, and Bloodwise. We are grateful for the technical assistance and advice of Adaptive Biotechnologies and of Jon Harris and Jan Soetaert from the Nikon Imaging Centre at Kings' College London.

Authorship

WT, SD, and AP conceived the research, analyzed data and prepared the manuscript. WT conducted most experimental work. EP contributed some experimental work. JS DY PP and RM provided specimens, clinical correlation and assisted in the preparation of the manuscript and helped develop and refine the experimental and analytical techniques. MP assisted in interpreting and analyzing the TCR repertoire. EP performed additional staining and microscopy. All authors contributed to and agreed the final manuscript.

Disclosures:

SD discloses consultancy fees and honoraria from Gilead.

WT discloses consultancy fees and honoraria from Roche and Gilead.

RM discloses consultancy fees and honoraria from Roche.

References

1. Harris N, Swerdlow S, Jaffe E, et al. WHO Classification of Tumours of Haematopoietic and Lymphoid Tissues, 4th edn. 4th ed. Lyon: International Agency for Research on Cancer, 2008.
2. Marafioti T, Copie-Bergman C, Calaminici M, et al. Another look at follicular lymphoma: immunophenotypic and molecular analyses identify distinct follicular lymphoma subgroups. Histopathology. 2013;62(6):860-875.
3. Ardeshna KM, Smith P, Norton A, et al. Long-term effect of a watch and wait policy versus immediate systemic treatment for asymptomatic advanced-stage non-Hodgkin lymphoma: a randomised controlled trial. Lancet. 2003;362(9383):516-522.
4. Montoto S, Davies AJ, Matthews J, et al. Risk and clinical implications of transformation of follicular lymphoma to diffuse large B-cell lymphoma. J Clin Oncol. 2007;25(17):2426-2433.
5. Ame-Thomas P, Tarte K. The yin and the yang of follicular lymphoma cell niches: role of microenvironment heterogeneity and plasticity. Semin Cancer Biol. 2014;24:23-32.
6. de Jong D, Koster A, Hagenbeek A, et al. Impact of the tumor microenvironment on prognosis in follicular lymphoma is dependent on specific treatment protocols. Haematologica. 2009;94(1):70-77.
7. Farinha P, Al-Tourah A, Gill K, Klasa R, Connors JM, Gascoyne RD. The architectural pattern of FOXP3-positive T-cells in follicular lymphoma is an independent predictor of survival and histologic transformation. Blood. 2010;115(2):289-295.
8. Farinha P, Masoudi H, Skinnider BF, et al. Analysis of multiple biomarkers shows that lymphoma-associated macrophage (LAM) content is an independent predictor of survival in follicular lymphoma (FL). Blood. 2005;106(6):2169-2174.
9. Dave SS, Wright G, Tan B, et al. Prediction of survival in follicular lymphoma based on molecular features of tumor-infiltrating immune cells. N Engl J Med. 2004;351(21):2159-2169.
10. Glas AM, Knoops L, Delahaye L, et al. Gene-expression and immunohistochemical study of specific T-cell subsets and accessory cell types in the transformation and prognosis of follicular lymphoma. J Clin Oncol. 2007;25(4):390-398.
11. Yang ZZ, Novak AJ, Stenson MJ, Witzig TE, Ansell SM. Intratumoral CD4+CD25+ regulatory T-cell-mediated suppression of infiltrating CD4+ T-cells in B-cell non-Hodgkin lymphoma. Blood. 2006;107(9):3639-3646.
12. Kiaii S, Clear AJ, Ramsay AG, et al. Follicular lymphoma cells induce changes in T-cell gene expression and function: potential impact on survival and risk of transformation. J Clin Oncol. 2013;31(21):2654-2661.
13. Lee AM, Clear AJ, Calaminici M, et al. Number of CD4+ cells and location of forkhead box protein P3-positive cells in diagnostic follicular lymphoma tissue microarrays correlates with outcome. J Clin Oncol. 2006;24(31):5052-5059.
14. Wahlin BE, Aggarwal M, Montes-Moreno S, et al. A unifying microenvironment model in follicular lymphoma: outcome is predicted by programmed death-1--positive, regulatory, cytotoxic, and helper T-cells and macrophages. Clin Cancer Res. 2010;16(2):637-650.
15. Carreras J, Lopez-Guillermo A, Roncador G, et al. High numbers of tumor-infiltrating programmed cell death 1-positive regulatory lymphocytes are associated with improved overall survival in follicular lymphoma. J Clin Oncol. 2009;27(9):1470-1476.

16. Richendollar BG, Pohlman B, Elson P, Hsi ED. Follicular programmed death 1-positive lymphocytes in the tumor microenvironment are an independent prognostic factor in follicular lymphoma. Hum Pathol. 2011;42(4):552-557.
17. Rolf J, Bell SE, Kovesdi D, et al. Phosphoinositide 3-kinase activity in T-cells regulates the magnitude of the germinal center reaction. J Immunol. 2010;185(7):4042-4052.
18. King C. New insights into the differentiation and function of T follicular helper cells. Nat Rev Immunol. 2009;9(11):757-766.
19. Crotty S. T follicular helper cell differentiation, function, and roles in disease. Immunity. 2014;41(4):529-542.
20. Linterman MA, Liston A, Vinuesa CG. T-follicular helper cell differentiation and the co-option of this pathway by non-helper cells. Immunol Rev. 2012;247(1):143-159.
21. Fazilleau N, Mark L, McHeyzer-Williams LJ, McHeyzer-Williams MG. Follicular helper T-cells: lineage and location. Immunity. 2009;30(3):324-335.
22. Yu D, Rao S, Tsai LM, et al. The transcriptional repressor BCL6 directs T follicular helper cell lineage commitment. Immunity. 2009;31(3):457-468.
23. Allen CD, Okada T, Cyster JG. Germinal-center organization and cellular dynamics. Immunity. 2007;27(2):190-202.
24. Pangault C, Ame-Thomas P, Ruminy P, et al. Follicular lymphoma cell niche: identification of a preeminent IL-4-dependent T(FH)-B cell axis. Leukemia. 2010;24(12):2080-2089.
25. Ame-Thomas P, Le Priol J, Yssel H, et al. Characterization of intratumoral follicular helper T-cells in follicular lymphoma: role in the survival of malignant B cells. Leukemia. 2012;26(5):1053-1063.
26. Yang ZZ, Grote DM, Ziesmer SC, Xiu B, Novak AJ, Ansell SM. PD-1 expression defines two distinct T-cell sub-populations in follicular lymphoma that differentially impact patient survival. Blood Cancer J. 2015;5:e281.
27. Ame-Thomas P, Hoeller S, Artchounin C, et al. CD10 delineates a subset of human IL-4 producing follicular helper T-cells involved in the survival of follicular lymphoma B cells. Blood. 2015;125(15):2381-2385.
28. Pandey S, Mourcin F, Marchand T, et al. IL-4/CXCL12 loop is a key regulator of lymphoid stroma function in follicular lymphoma. Blood. 2017;129(18):2507-2518.
29. Ansell SM, Lesokhin AM, Borrello I, et al. PD-1 blockade with nivolumab in relapsed or refractory Hodgkin's lymphoma. N Engl J Med. 2015;372(4):311-319.
30. Hawkes EA, Grigg A, Chong G. Programmed cell death-1 inhibition in lymphoma. Lancet Oncol. 2015;16(5):e234-245.
31. Westin JR, Chu F, Zhang M, et al. Safety and activity of PD1 blockade by pidilizumab in combination with rituximab in patients with relapsed follicular lymphoma: a single group, open-label, phase 2 trial. Lancet Oncol. 2014;15(1):69-77.
32. Gopal AK, Kahl BS, de Vos S, et al. PI3Kdelta inhibition by idelalisib in patients with relapsed indolent lymphoma. N Engl J Med. 2014;370(11):1008-1018.
33. Robins HS, Campregher PV, Srivastava SK, et al. Comprehensive assessment of T-cell receptor beta-chain diversity in alphabeta T-cells. Blood. 2009;114(19):4099-4107.
34. Yousfi Monod M, Giudicelli V, Chaume D, Lefranc MP. IMGT/JunctionAnalysis: the first tool for the analysis of the immunoglobulin and T-cell receptor complex V-J and V-D-J JUNCTIONs. Bioinformatics. 2004;20 Suppl 1:i379-385.

35. Haynes NM, Allen CDC, Lesley R, Ansel KM, Killeen N, Cyster JG. Role of CXCR5 and CCR7 in Follicular Th Cell Positioning and Appearance of a Programmed Cell Death Gene-1 High Germinal Center-Associated Subpopulation. J Immunol. 2007;179(8):5099-5108.
36. Andorsky DJ, Yamada RE, Said J, Pinkus GS, Betting DJ, Timmerman JM. Programmed death ligand 1 is expressed by non-hodgkin lymphomas and inhibits the activity of tumor-associated T-cells. Clin Cancer Res. 2011;17(13):4232-4424.
37. Kupfer A, Kupfer H. Imaging immune cell interactions and functions: SMACs and the Immunological Synapse. Semin Immunol. 2003;15(6):295-300.
38. Sherwood AM, Emerson RO, Scherer D, et al. Tumor-infiltrating lymphocytes in colorectal tumors display a diversity of T-cell receptor sequences that differ from the T-cells in adjacent mucosal tissue. Cancer Immunol Immunother. 2013;62(9):1453-1461.
39. Nazarov VI, Pogorelyy MV, Komech EA, et al. tcR: an R package for T-cell receptor repertoire advanced data analysis. BMC Bioinformatics. 2015;16:175.
40. Myklebust JH, Irish JM, Brody J, et al. High PD-1 expression and suppressed cytokine signaling distinguish T-cells infiltrating follicular lymphoma tumors from peripheral T-cells. Blood. 2013;121(8):1367-1376.
41. Victora GD, Nussenzweig MC. Germinal centers. Annu Rev Immunol. 2012;30:429-457.
42. Ramsay AG, Clear AJ, Kelly G, et al. Follicular lymphoma cells induce T-cell immunologic synapse dysfunction that can be repaired with lenalidomide: implications for the tumor microenvironment and immunotherapy. Blood. 2009;114(21):4713-4720.
43. Barcia C, Thomas CE, Curtin JF, et al. In vivo mature immunological synapses forming SMACs mediate clearance of virally infected astrocytes from the brain. J Exp Med. 2006;203(9):2095-2107.
44. Pasqualucci L, Bhagat G, Jankovic M, et al. AID is required for germinal center-derived lymphomagenesis. Nat Genet. 2008;40(1):108-112.
45. Pasqualucci L, Khiabanian H, Fangazio M, et al. Genetics of follicular lymphoma transformation. Cell Rep. 2014;6(1):130-140.
46. Best K, Oakes T, Heather JM, Shawe-Taylor J, Chain B. Computational analysis of stochastic heterogeneity in PCR amplification efficiency revealed by single molecule barcoding. Sci Rep. 2015;5:14629.

Figure legends

Figure 1. Distribution of CD4^{pos} PD-1^{pos} ICOS^{pos} cells in normal germinal centers and follicular lymphoma. (**a1**) Low power view of germinal centers in a reactive lymph node showing CD4^{pos} (red) T-cells mainly outside the germinal center. A population of cells within the GCs co-express PD-1 (white) and ICOS (green). (**a2**) The area highlighted by the white rectangle has been enlarged showing the distribution of CD4/PD1/ICOS^{pos} cells in a normal germinal center where they are mainly polarized to the light zone (**a3**) Intersecting binary

layer of image (a1) showing CD4/PD-1/ICOS^{pos} cells (magenta) in germinal centers. DAPI staining (blue) highlights cell nuclei. (**a4**) High power view of the intersecting CD4/PD-1/ICOS^{pos} binary layer. (**b1**) Representative image of follicular lymphoma lymph node showing CD4^{pos} (red) T-cells mainly outside the follicles but a population within the follicles co-express PD-1 (white) and ICOS (green). (**b2**) Same image as **(b1)** showing only DAPI (blue) and the intersecting binary layer of CD4/PD-1/ICOS^{pos} cells (magenta) which are restricted to the follicles where they are located predominantly in a peri-follicular pattern. Scale bars represent 100µm. (**c**) There was no significant difference in the proportion of CD4^{pos} cells co-expressing PD-1 and ICOS in normal and neoplastic follicles. There was a small but significant increase in CD4/PD-1/ICOS^{pos} cells in the interfollicular compartment of follicular lymphoma compared to the same area zone of reactive LNs. Horizontal lines represent median, boxes represent interquartile range, 'whiskers' represent range. **(d)** Representative, magnified image showing BLC6 expression in T-cells in neoplastic follicles. Four CD3^{pos} (blue) cells are shown, three are positive for the transcription factor BCL6 (red) and these are also PD-1^{pos} (white) and ICOS^{pos} (green), indicated with white arrows. One CD3^{pos} cell is negative for BCL6 (green arrow), and this cell does not express PD-1 or ICOS. Overall 89.6% (88.3-91.8) of CD3^{pos}PD1^{pos}ICOS^{pos} cells express BCL6.

Figure 2. Close physical association between Ki67^{pos} B-cells and T_{FH} in normal germinal center light zones. (**a1**) Representative low power image showing polarization of Ki67^{pos} cells to the dark zones of normal germinal centers. Ki67 (red), PD-1 (white), ICOS (green), DAPI (blue). Scale bar represents 100µm. The area highlighted by the white rectangle is shown in high power in (**a2**). (**a3**) The close association between Ki67^{pos} FL cells (red) and PD-1^{Hi} cells (white) is shown in the light zone of another follicle whereas in the dark zone

there is less interaction between Ki67^{pos} cells and PD-1^{Hi} T-cells. The scale bar represents 25µm. (**b1**) Using a different 4-colour panel, the Ki67^{pos} cells (blue) were confirmed as CD20^{pos} B-cells (red) and the PD-1^{Hi} cells (white) were confirmed as CD3^{pos} T-cells (green). The scale bar represents 100µm and the area highlighted by the white rectangle has been magnified in (**b2**). Images representative of n=13 images from n=4 reactive lymph node samples. (**c**) Contingency table showing that Ki67^{pos} B-cells are significantly more likely to be in contact with T_{FH} than Ki67^{neg} B-cells in normal germinal center light zones, as quantified by manual visual assessment. For all samples analyzed together (n = 5, Fisher's exact test P <0.0001).

Figure 3. Ki67^{pos} cells are in close proximity to T_{FH} in follicular lymphoma lymph nodes. (**a1**) Representative image of a neoplastic follicle showing Ki67^{pos} cells (green) in close proximity to CD4^{pos} (red), PD-1^{Hi} (white) T-cells. The scale bar represents 25µm. (**a2**) Binary image of (**a1**), the binary layers of Ki67 (green) and the CD4-PD-1^{Hi} intersection (magenta) are shown highlighting the close association of Ki67^{pos} cells to PD-1^{Hi} T-cells. (**b1**) Representative image demonstrating that the majority of the PD-1^{Hi} cells in contact with Ki67^{pos} cells (red) are also positive for ICOS (green). (**b2**) This is highlighted in the binary layer 3D reconstruction of the same image, PD-1/ICOS^{pos} (magenta) and Ki67 (green). Images representative of n=100 images from n=23 follicular lymphoma samples (4a), n=43 images from n=13 samples (4b). **(c1)** Ki67 = blue, CD20 = red, PD-1 = white, CD3 = green. Low power image (x10) showing Ki67^{pos} and Ki67^{neg} CD20^{pos} B-cell co-localisation with PD1^{Hi} CD3^{pos} T-cells in FL. Within the follicles there are areas of low proliferation (low Ki67 - blue) where there are few PD1^{Hi} (white) CD3^{pos} T-cells (green) - area highlighted by yellow oval, whereas in areas where

there is high Ki67, there are more $PD1^{Hi}$, $CD3^{pos}$ T-cells (area highlighted by white circle) and they are frequently in contact with $Ki67^{pos}$ $CD20^{pos}$ FL B-cells (scale bar = 100μm). **(c2)** High power image (x60) in which the close correlation of $Ki67^{pos}$ (blue) B-cells with $PD1^{Hi}$ (white) $CD3^{pos}$ (green) cells can be seen, whilst the $CD20^{pos}$ (red), $Ki67^{neg}$ cells are less frequently in contact with T_{FH} cells (scale bar = 50μm). **(c3)** contingency tables showing that $Ki67^{pos}$ B-cells are significantly more likely to be in contact with T_{FH} than $Ki67^{neg}$ B-cells in follicular lymphoma (For all samples analyzed together (n=25 images from n=7 follicular lymphoma specimens) Chi squared 595, $P < 0.0001$.

Figure 4. Association between Ki67 and number of T_{FH} in follicular lymphoma. (**a**) The area of the Ki67 binary layer correlates closely with the number of $Ki67^{pos}$ cells automatically counted (left) and the area of the Ki67 binary layer is significantly higher in grade 3a or 3b disease than in grade 1-2 disease (right), n=99 images from n=23 samples. (**b**) The number of $Ki67^{pos}$ cells correlates closely with the number of $PD1^{pos}ICOS^{pos}$ cells (left) and there are significantly more T_{FH} (as represented by increased area of PD1/ICOS intersection) in grade 3a and 3b disease than in grade 1-2 disease (right), n=42 images from n=13 samples. (**c**) The degree of T_{FH} – Ki67 interaction is weakly associated with the number of $Ki67^{pos}$ cells (left), and the proportion of $Ki67^{pos}$ cells in contact with T_{FH} does not differ significantly according to histological grade disease (right) (n=42 images from n=13 samples).

Figure 5. Close contact between $Ki67^{pos}$ cells and T_{FH} in follicular lymphoma: Evidence for immune synapse formation. (**a1**) A $Ki67^{pos}$ cell (red) is seen to be in contact with 4 $PD\text{-}1^{pos}$ (white) $ICOS^{pos}$ (green) cells simultaneously. The $PD\text{-}1^{pos}ICOS^{pos}$ cells are closely associated with the $Ki67^{pos}$ cell. (**a2**) Binary layer image of **a1**, the binary layers of Ki67 (red) and PD-1/ICOS intersection (magenta) are shown highlighting the close spatial association. Scale

bars represent 10µm. (**b1**) The T_{FH} cells form projections encompassing the $Ki67^{pos}$ cells. Scale bar represents 10µm. The perimeter of the T_{FH} cell has been highlighted by the red dotted line and the intensity of CD4, PD-1 and ICOS have been measured around this line. CD4, PD1 and ICOS are more concentrated at the pole in contact with the $Ki67^{pos}$ cell as seen in the representative graph of intensity of expression around the dotted line, the area of cell contact is highlighted in the shaded area (**b2**). (**b3**) CD4, PD1, and ICOS all have significantly higher intensity of expression at the sites of cell contact than at the opposite pole, paired t tests, n=61 cell contacts, from highly magnified images in 9 follicular lymphoma specimens stained with CD4/PD-1/Ki67, or PD-1/ICOS/Ki67.

Figure 6. Evidence of T-cell receptor repertoire restriction in follicular lymphoma. (**a**) The clonality of the T-cell receptors in intrafollicular areas was higher than in the interfollicular compartment in all cases examined, horizontal bars represent mean of all samples, median clonality 0.062 vs 0.049 respectively, Mann Whitney, P = 0.0317. (**b**) Summary of T-cell receptor repertoire data showing the proportion of the total population accounted for by high frequency clones in the follicular and interfollicular regions of follicular lymphoma lymph nodes. In each case, the more frequent clones predominate in the follicular regions compared to the interfollicular areas. (**c**) The level of overlap of clonotypes between follicular and interfollicular compartments for all clones in paired samples (all clones) and for the 100 most frequent clones (top 100 clones). Horizontal bars represent the mean overlap (0.125 for all clones and 0.22 for top 100 clones)

Figure 1

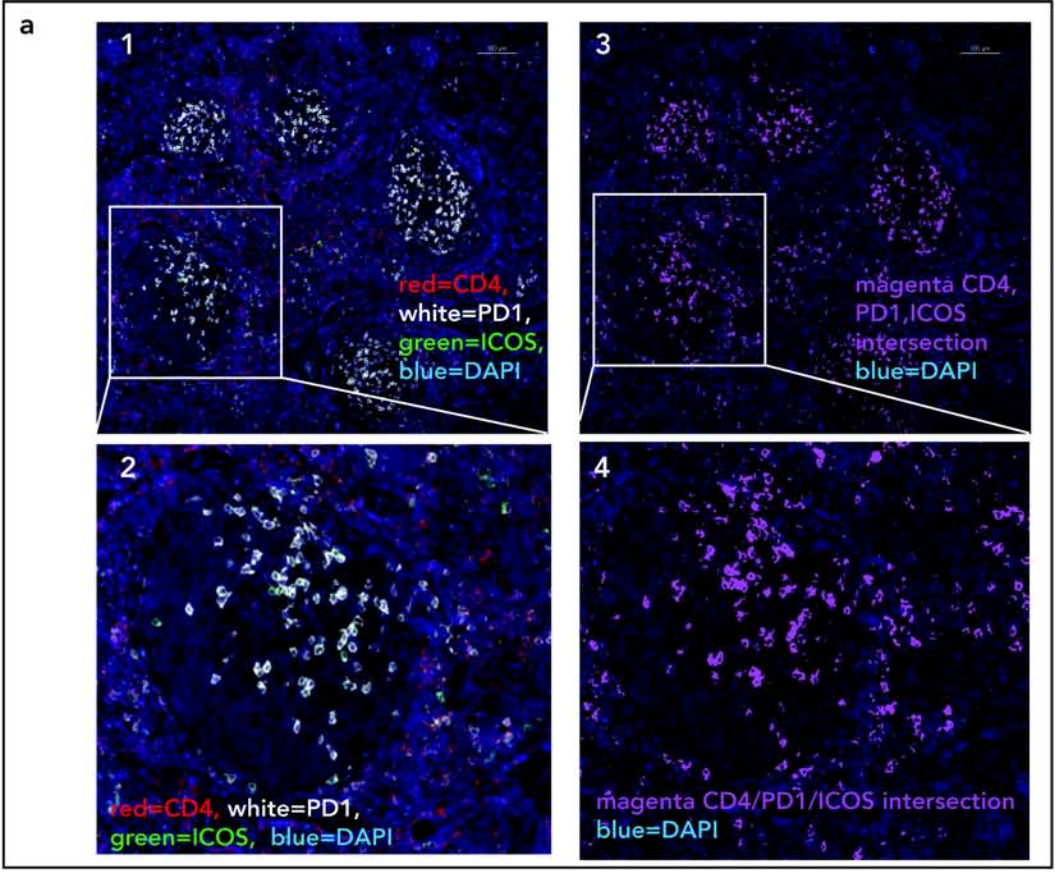
a
1
red=CD4,
white=PD1,
green=ICOS,
blue=DAPI
3
magenta CD4,
PD1,ICOS
intersection
blue=DAPI
2
red=CD4, white=PD1,
green=ICOS, blue=DAPI
4
magenta CD4/PD1/ICOS intersection
blue=DAPI

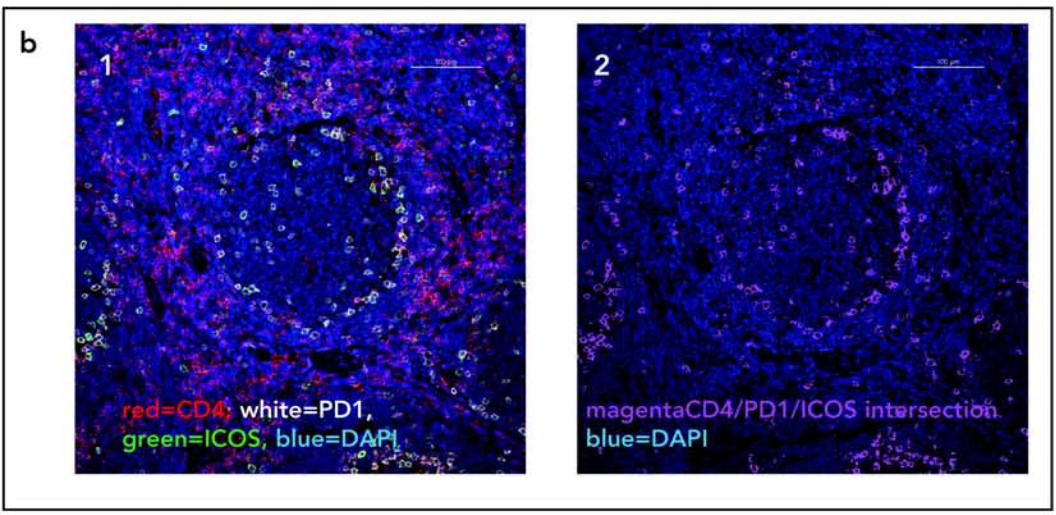
b
1
red=CD4; white=PD1,
green=ICOS, blue=DAPI
2
magentaCD4/PD1/ICOS intersection
blue=DAPI

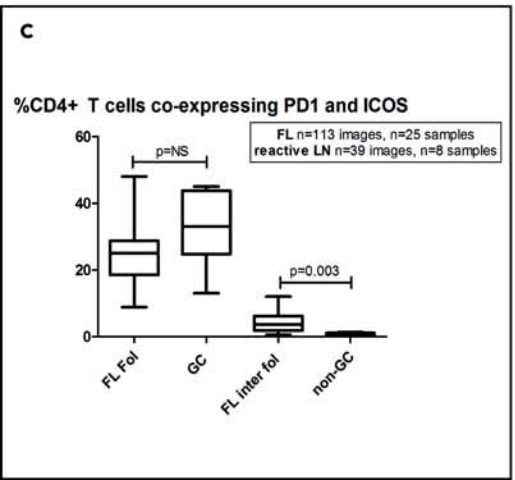
c
%CD4+ T cells co-expressing PD1 and ICOS
FL n=113 images, n=25 samples
reactive LN n=39 images, n=8 samples
60
40
20
0
p=NS
p=0.003
FL Fol
GC
FL inter fol
non-GC

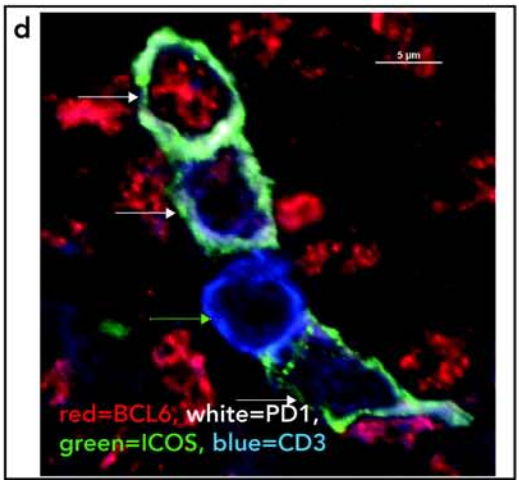
d
5 µm
red=BCL6; white=PD1,
green=ICOS, blue=CD3

a

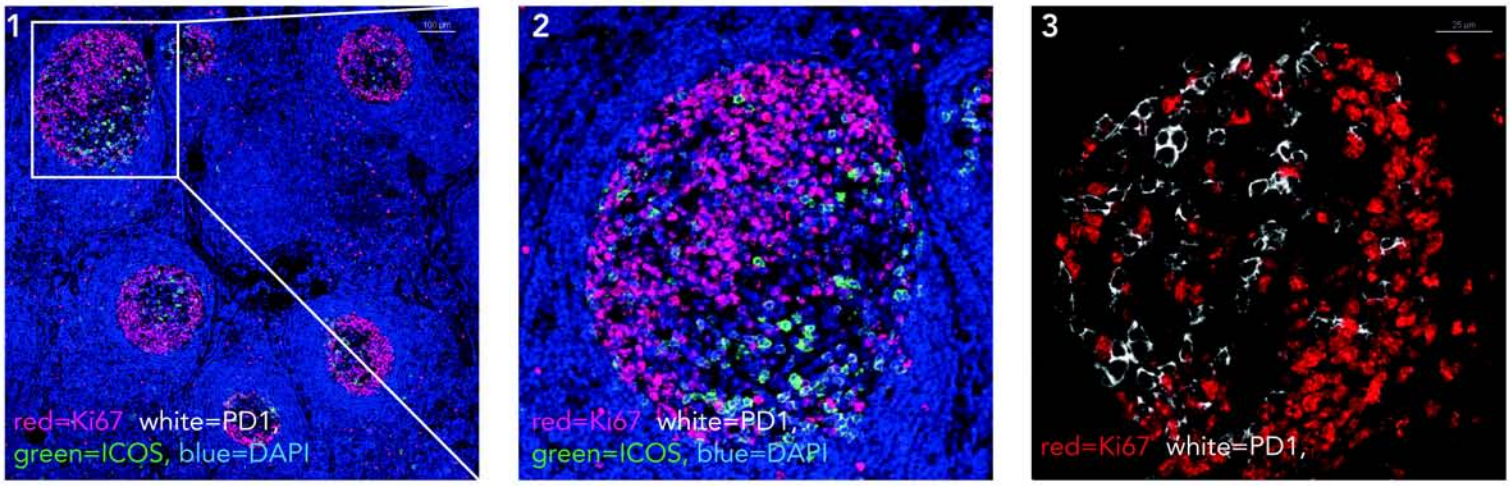

b

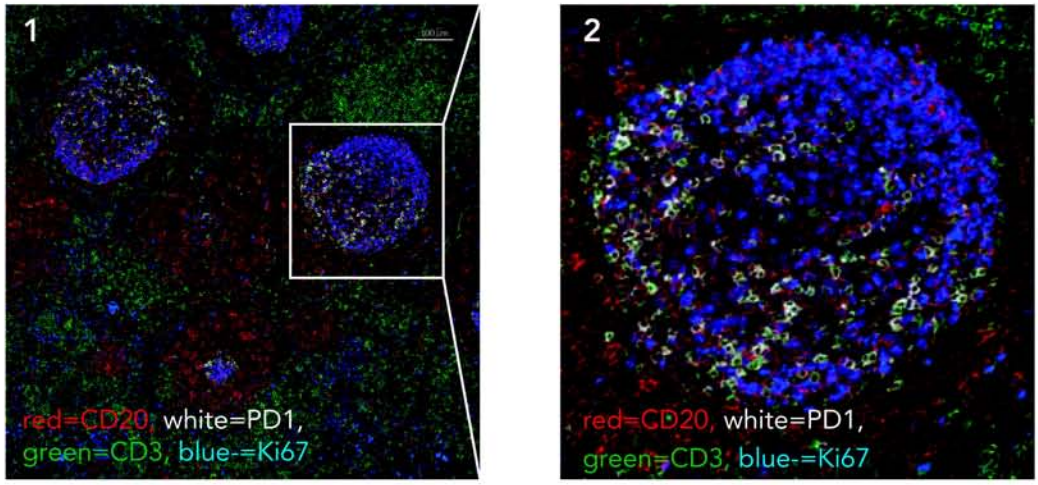

c

GCs	$Ki67^{POS}$ B-cells	$Ki67^{NEG}$ B-cells	Total
In contact with T_{FH}	125	67	192
Not in contact with T_{FH}	49	72	121
Total	174	139	313

Fishers exact test, p=<0.0001

a

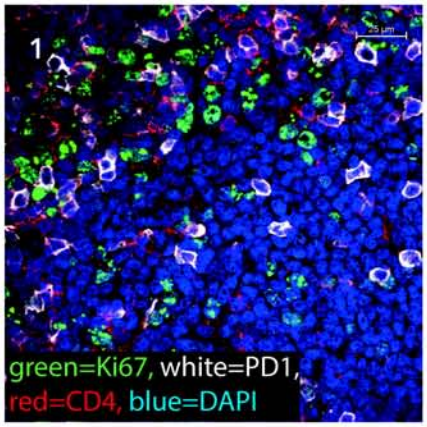

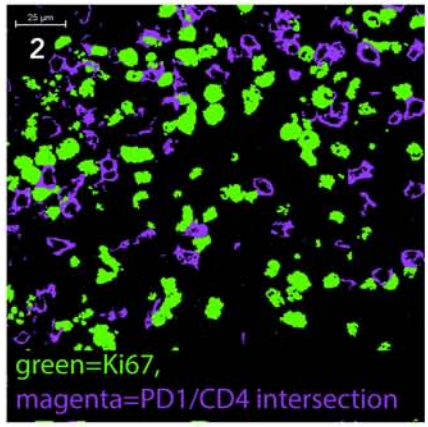

b

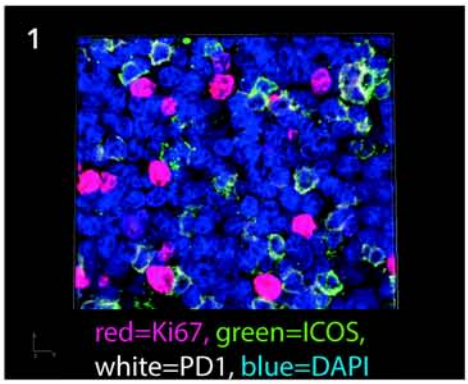

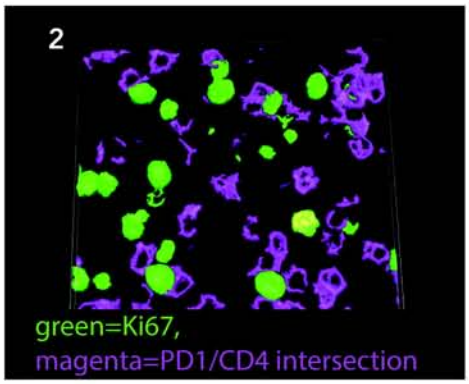

c

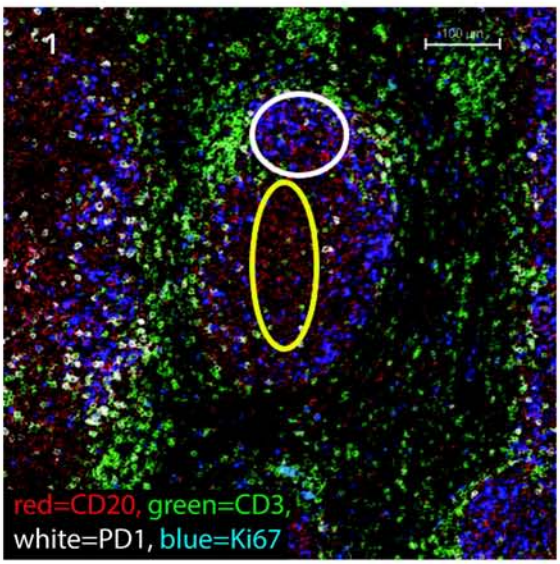

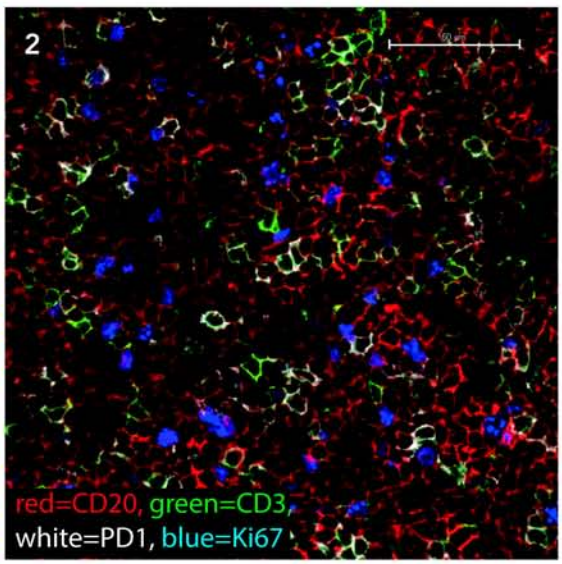

FL follicles	$Ki67^{POS}$ B-cells	$Ki67^{NEG}$ B-cells	Total
In contact with T_{FH}	877	552	1429
Not in contact with T_{FH}	604	2045	2649
Total	1481	2597	4078

Chi squared 595, p=<0.0001

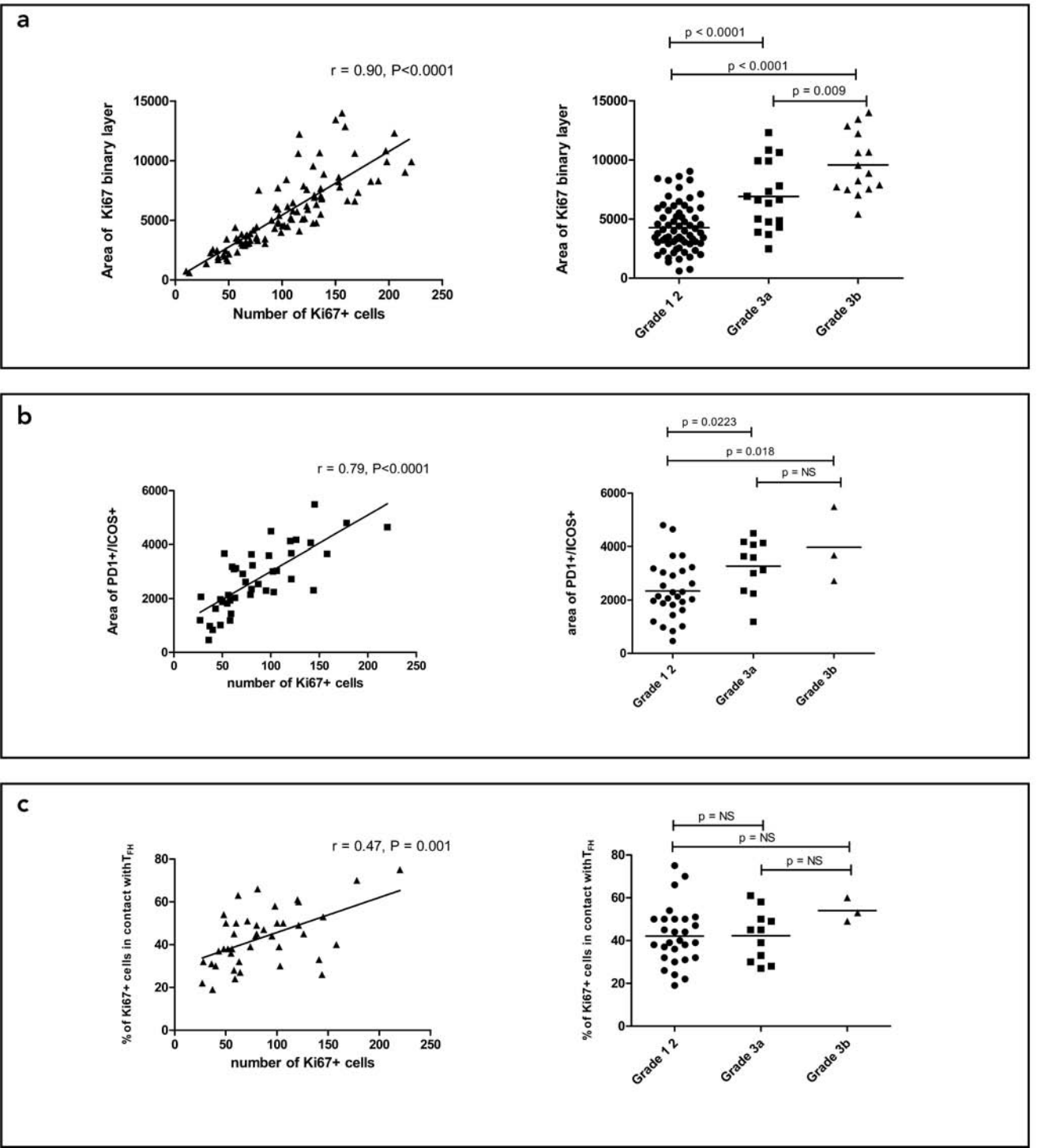
a
r = 0.90, P<0.0001
Area of Ki67 binary layer
Number of Ki67+ cells
p < 0.0001
p < 0.0001
p = 0.009
Area of Ki67 binary layer
Grade 1 2
Grade 3a
Grade 3b
b
r = 0.79, P<0.0001
Area of PD1+/ICOS+
number of Ki67+ cells
p = 0.0223
p = 0.018
p = NS
area of PD1+/ICOS+
Grade 1 2
Grade 3a
Grade 3b
c
r = 0.47, P = 0.001
% of Ki67+ cells in contact with TFH
number of Ki67+ cells
p = NS
p = NS
p = NS
% of Ki67+ cells in contact with TFH
Grade 1 2
Grade 3a
Grade 3b

Figure 5

a

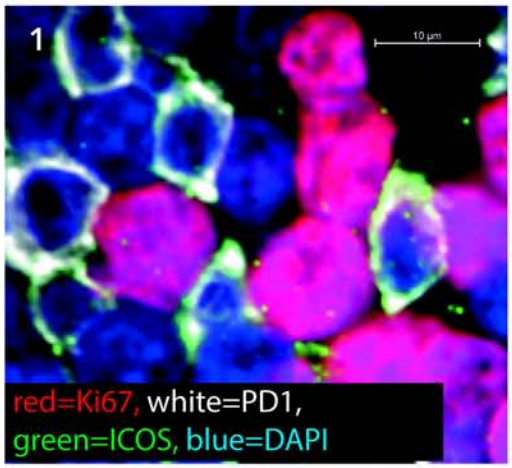
1
10 µm
red=Ki67, white=PD1,
green=ICOS, blue=DAPI

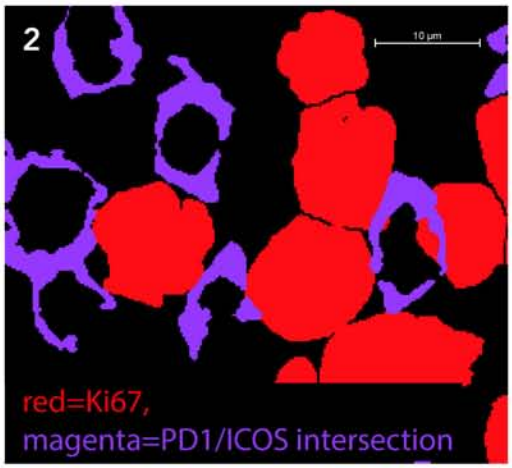
2
10 µm
red=Ki67,
magenta=PD1/ICOS intersection

b

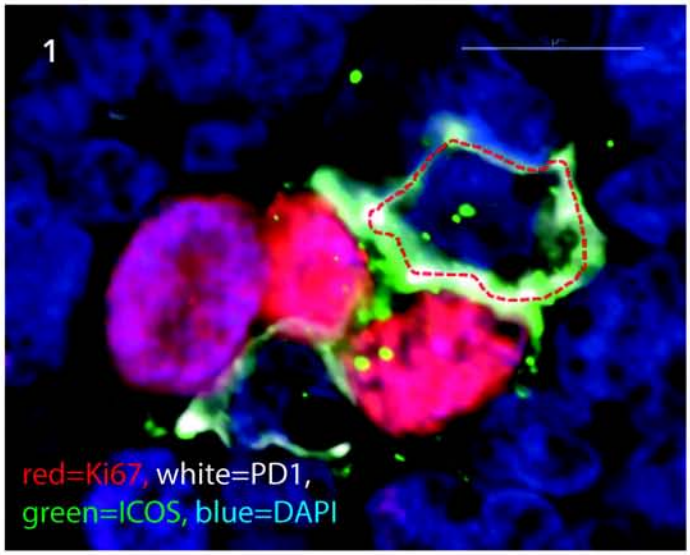
1
red=Ki67, white=PD1,
green=ICOS, blue=DAPI

3

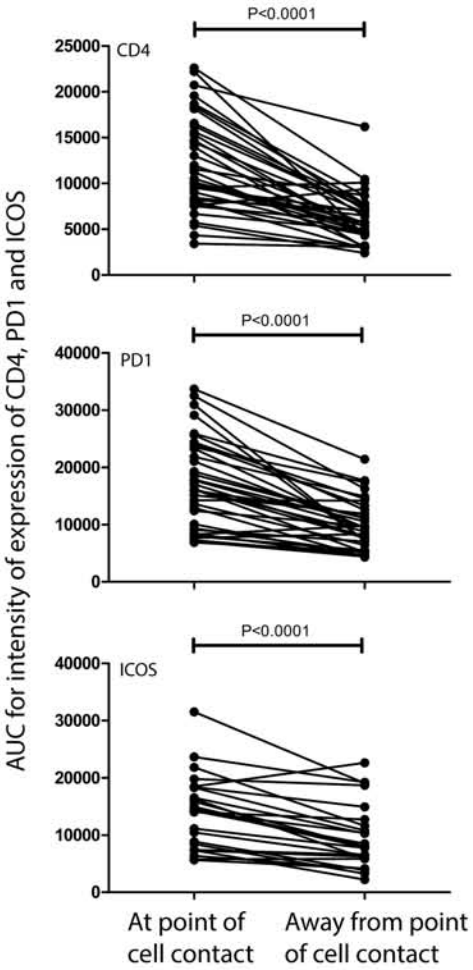
P<0.0001
CD4
25000
20000
15000
10000
5000
0
P<0.0001
PD1
40000
30000
20000
10000
0
P<0.0001
ICOS
40000
30000
20000
10000
0
AUC for intensity of expression of CD4, PD1 and ICOS
At point of cell contact
Away from point of cell contact

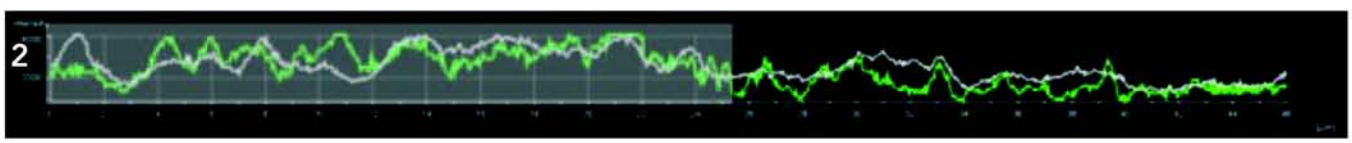
2

a

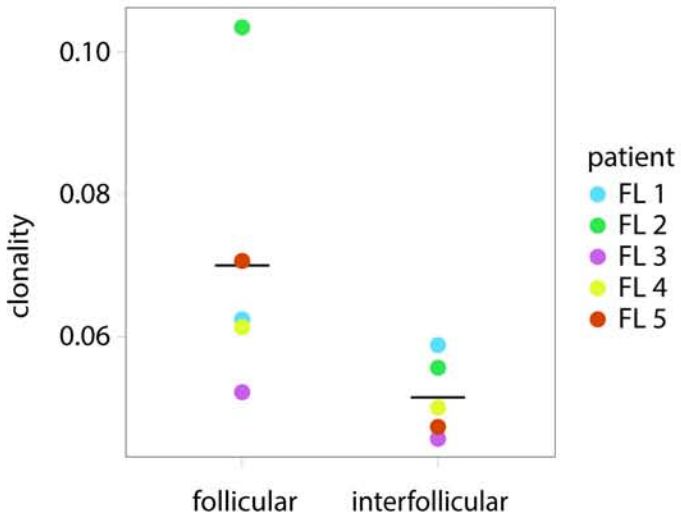
0.10
0.08
0.06
clonality
follicular
interfollicular
patient
FL 1
FL 2
FL 3
FL 4
FL 5

b

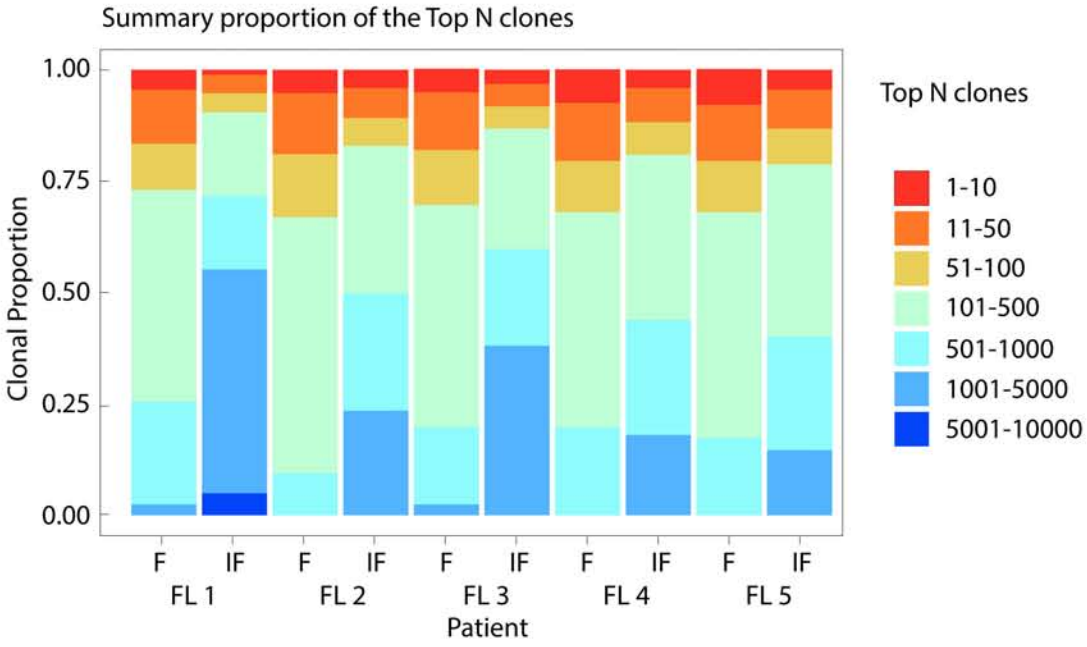
Summary proportion of the Top N clones
1.00
0.75
0.50
0.25
0.00
Clonal Proportion
F
IF
FL 1
FL 2
FL 3
FL 4
FL 5
Patient
Top N clones
1-10
11-50
51-100
101-500
501-1000
1001-5000
5001-10000

c

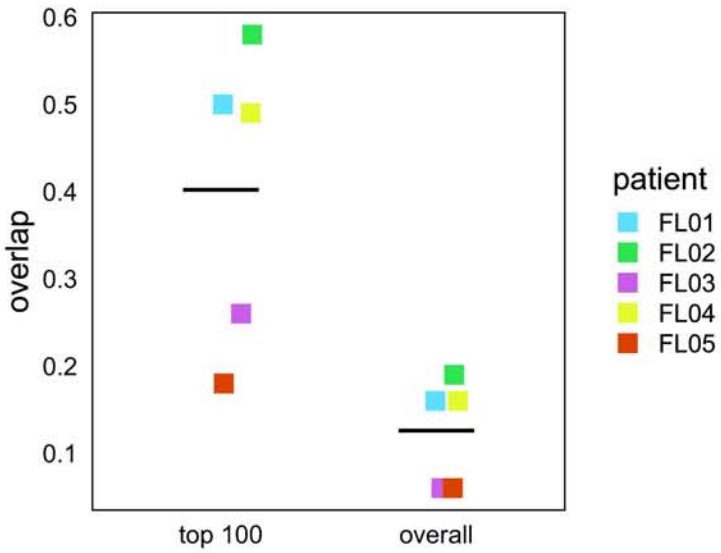
0.6
0.5
0.4
0.3
0.2
0.1
overlap
top 100
overall
patient
FL01
FL02
FL03
FL04
FL05

Supplementary Material

Preparation of slides for immunofluorescent confocal microscopy

FFPE LN blocks were cut into sections of 4µm or 12µm thickness, mounted onto Poly-L-Lysine coated slides and deparaffinized in xylene followed by rehydration in graded ethanol. Heat induced epitope retrieval was performed in pH 6.1 citrate buffer with 0.05% Tween 20 in a pressure cooker for 3 minutes. Sections were rehydrated before blocking in 5% normal donkey serum (Jackson ImmunoResearch, West Grove, Pennsylvania, USA) for 1 hour. Sections were then incubated with combinations of 3 or 4 primary antibodies with 0.025% Triton X-100 for 12 hours at 4°C in a humidified chamber. The antibodies used and their concentrations are listed in Table S3. The antibodies used in each combination were raised in different species to facilitate detection by species-specific secondary antibodies. After primary antibody incubation, slides were washed and then incubated with the appropriate combination of fluorescently-conjugated secondary antibodies and 4',6-diamidino-2-phenylindole dihydrochloride (DAPI) (Cell Signaling Technology, Danvers, USA) if a nuclear stain was required. Sections were mounted with coverslips using ProLong Gold Antifade mounting medium (Invitrogen, Carlsbad, California, USA).

Negative controls were run in parallel with all staining to ensure that the fluorescence detected was not due to non-specific binding of the secondary antibodies or tissue autofluorescence. Positive controls were reactive LNs or tonsil tissue. Additional controls were performed to ensure there was no spectral overlap of the fluorescently-conjugated antibodies.

Image acquisition

All images were acquired on a Nikon Eclipse Ti-E upright microscope equipped with Nikon A1R Si confocal imaging system and lasers emitting at 405nm, 488nm, 561nm, and 642nm (Nikon Corporation, Tokyo, Japan). Low power images were obtained with a Pan Fluor x10 objective and high power images with a Pan Apo oil immersion x60 objective. To maintain consistency and to permit comparative analyses, all images were acquired on the same microscope and laser power, photo multiplier tube (PMT) gain, pixel dwell time, pin hole size, optical section thickness, offset, and filter settings were kept the same for analysis of paired control slides. These settings were maintained as closely as possible for all similarly stained sections but small differences in the thickness of tissue, quality of fixation, and the age of the specimen affected the strength of antibody binding, fluorescence and autofluorescence and accordingly, laser power, PMT gain, and offset were optimised for individual sections. 3-5 high power images (x60 objective) were obtained and analysed from representative follicular and interfollicular areas of each section.

Image analysis

Binary layers were generated for each channel by setting thresholds to define which areas of an image were positive signal and included in the binary layer, and which areas were negative or background and excluded from the binary layer. Thresholding was performed on the basis of intensity of fluorescence in each channel and a size restriction to reduce false positive signal from small areas of autofluorescence. Large areas of autofluorescence or artefact from blood vessels or formalin crystals were deleted manually from the binary layers.

Generating binary layers for each channel permitted the accurate, automated quantification of the area of positive signal in an image, and the analysis of cellular co-localization. Areas

where combinations of antigens were expressed were calculated by defining 'intersecting' binary layers where the signal in 2 or more channels overlapped. This was used for example for identifying $CD4^{pos}$ cells that co- expressed PD-1 and ICOS; the proportion of $CD4^{pos}$ cells co-expressing these antigens was calculated by dividing the area of the CD4 PD-1 ICOS intersecting binary layer by the total area of the CD4 layer.

The proportion of proliferating cells in contact with T_{FH} cells was calculated by defining individual cells in the Ki67 binary layer and automatically quantifying the proportion that were in direct contact with the intersecting binary layer of CD4 PD-1 or PD-1 ICOS (Figure S1).

For the analysis of $CD20^{pos}$ cells that were in contact with T_{FH}, manual, visual analysis had to be performed as the diffuse pattern of CD20 staining and the closely packed nature of $CD20^{pos}$ cells meant that the automated analysis software was unable to reliably distinguish individual $CD20^{pos}$ cells that were not $Ki67^{pos}$. To perform this, images were thresholded according to the method described above and binary layers of the intersecting CD3 and PD1 binary layers were created. A grid was superimposed over the image to aid visual assessment and to help ensure that each area of the image was inspected. A 'taxonomy tool' within the NIS elements software package was then used for the manual counting of $Ki67^{pos}$ and $Ki67^{neg}$ $CD20^{pos}$ B-cells that were, or were not in contact with T_{FH}.

Due to the manual visual assessment of these images, two separate investigators analysed a subset of these images in order to identify and reduce operator bias. The two investigators were blinded to each other's results. There was no significant difference in number of $Ki67^{pos}$ cells counted by observer, the number of cells in contact with T_{FH} was also concordant between operators.

Manual measurement was also used for analysis of BCL6 and FOXP3 images.

Images have been optimized for contrast using contrast settings and Look Up Tables (LUTs) and, where appropriate, magnification has been performed, no further image enhancement or manipulation has been used.

DNA extraction and TCR sequencing

Equivalent areas of tissue were dissected from follicular and interfollicular areas. Genomic DNA was extracted using the miniDNA extraction kit (Qiagen, Venlo, Netherlands) according to the manufacturer's instructions.

TCR repertoire data analysis

Clonality index

The clonality index was derived from Shannon's entropy, a measure of the certainty with which the identity of a clone selected randomly from a population of different clones can be predicted.(1) It is influenced by both the total number of different clones and the diversity of the population. Using this measure, a population or sample containing only one clone would have an entropy of 0, whilst a completely polyclonal population, in which all clones are equally frequent, would have a Shannon's entropy equal to the logarithm of the number of unique sequences. To allow populations containing different numbers of unique clones to be compared, the entropy was normalized by dividing by the logarithm of the number of unique clones present. The clonality index corresponds to the reciprocal of the normalized entropy so that a monoclonal population gives a value of 1 and a polyclonal population 0.

Similarity index

The overlap between two populations was captured by the Jaccard index; the number of shared TCR sequences divided by the total number of distinct sequences in the two populations

Statistical analysis

Statistical analysis was performed using GraphPad Prism software v5 (GraphPad Software Inc, La Jolla, California, USA). Normally distributed values are presented as the mean (+/- standard deviation), non-normally distributed values are presented as median (+/- interquartile range). Normally distributed variables were compared using two-tailed Students unpaired or paired t tests; non-normally distributed data were compared with Mann Whitney tests for unpaired and Wilcoxon paired rank test for paired data. Statistical significance was assumed when *P* was <0.05.

Contingency tables were used to determine whether $Ki67^{pos}$ cells were more likely than $Ki67^{neg}$ cells to be in contact with T_{FH}. Fisher's exact test was used to compare individual samples, for comparing total numbers of cells in multiple samples, Fisher's exact test was used for GCs, and Chi squared for FL.

For correlations e.g. between number of $Ki67^{pos}$ cells and number of $T_{FH,}$ Spearman non-parametric correlation coefficient was used.

Supplementary tables

Table S1: Clinical characteristics of FL patients

Sample	Age (years)	Gender	Grade	Stage	Disease status at biopsy	Prior therapy
FL001	68	Female	1	IV	relapse	R-CVP
FL002	88	Female	3b	I	untreated	not treated*
FL003	47	Male	2	IV	untreated	R-CVP
FL004	56	Male	2	IV	untreated	R-CHOP
FL005	45	Female	2	IV	untreated	R-CVP
FL006	41	Male	2	IV	untreated	R-CHOP + R
FL007	63	Female	3a	III	untreated	R-CHOP
FL008	60	Female	1	III	untreated	W&W
FL009	34	Female	3b	I	untreated	R-CHOP + RT
FL010	70	Female	2	III	relapse	R-CVP + R
FL011	58	Male	3b	III	untreated	R-CHOP
FL012	29	Male	2	IV	untreated	R-CVP
FL013	47	Female	1	IV	relapse	R-FC + ASCT
FL014	54	Male	2	III	untreated	W&W
FL015	57	Male	1	IV	untreated	R-CVP
FL016	32	Male	3a	IV	untreated	W&W
FL017	33	Male	1 - 2	IV	relapse	W&W
FL018	52	Male	1 - 2	IV	untreated	W&W
FL019	58	Male	3a	IV	relapse	R-bendamustine
FL020	38	Female	1 - 2	III	untreated	W&W
FL021	63	Female	1	III	untreated	W&W
FL022	88	Female	1	IV	relapse	R-CVP
FL023	62	Male	1 - 2	II	relapse	W&W
FL024	55	Female	3a	III	untreated	R-bendamustine
FL025	60	Male	3a	III	untreated	R-bendamustine

* too frail to receive treatment and died due to ischemic heart disease and FL 5 months after diagnosis

R-CVP = rituximab, cyclophosphamide, vincristine, prednisolone. R-CHOP = rituximab, cyclophosphamide, doxorubicin, vincristine, prednisolone. W&W = watch and wait. RT = radiotherapy. R-FC = rituximab, fludarabine, cyclophosphamide. R = rituximab. CR = complete response. PR = partial response. HSCT = hematopoietic stem cell transplantation.

Table S2: Clinical characteristics of patients with reactive lymph node biopsies

Sample	Age (years)	Gender
rLN01	29	Male
rLN02	1	Male
rLN03	35	Female
rLN04	40	Female
rLN05	27	Male
rLN06	53	Female
rLN07	25	Male
rLN08	54	Female

Table S3: Antibodies used for immunofluorescent labelling

Primary Antibodies

Target	Species	Manufacturer	Clone	Dilution
CD3	Rat	Abcam	CD3-12	1:200
ICOS	Rabbit	Abcam	SP98	1:100
Ki67	Rabbit	Abcam	Polyclonal	1:100
T-bet	Rabbit	Abcam	EPR9302	1:200
CD8	Rabbit	Abcam	EP1150Y	1:400
PD1	Goat	R&D systems	Polyclonal	1:50
Ki67	Mouse	Leica Novocastra	MM1	1:100
CD20cy	Mouse	Dako	L26	1:400
Bcl-6	Mouse	Dako	PG-B6p	1:50
CD4	Mouse	Leica Novocastra	4B12	1:50
AID	Mouse	Invitrogen	ZA001	1:200
PDL1	Rabbit	Spring Bioscience	SP142	1:200
FOXP3	Mouse	Abcam	236A/E7	1:100

Species-specific Fluorescently conjugated Secondary Antibodies (all raised in Donkey)

Target	Fluorochrome	Manufacturer	Dilution	Excitation Peak (nm)	Emission Peak (nm)
Rat IgG	DyLight 405	Jackson	1:200	400	421
Rabbit IgG	DyLight 405	Jackson	1:200	400	421
Rabbit IgG	Alexa Fluor 488	Jackson	1:200	493	519
Rat IgG	Alexa Fluor 488	Jackson	1:200	493	519
Mouse IgG	Alexa Fluor 555	Life Technologies	1:200	555	565
Goat IgG	Alexa Fluor 647	Jackson	1:200	651	667
Rat IgG	Alexa Flour 647	Jackson	1:200	651	667

Table S4. Number of unique TCR sequences in intra- and inter-follicular areas of FL LNs

Case no	input DNA (ng)		No of unique TCRs		Unique TCRs/ng input DNA	
	F	IF	F	IF	F	IF
	P=0.05		P=0.06*		P=0.06	
FL01	218	402	1270	3450	5.83	8.58
FL02	336	764	1054	2044	3.14	2.68
FL03	341	376	822	2236	2.41	5.95
FL04	370	653	1901	7214	5.14	11.05
FL05	310	377	1033	2008	3.33	5.33

F= follicular region, IF = interfollicular region. TCRs = unique productive nucleotide reads of T-cell receptor CDR3 region. Significance of differences assessed by paired t test or Wilcoxon paired rank test*.

Supplemental Figure Legends:

Figure S1. Example of triple staining of a reactive lymph node showing how binary layers are created. Ai, **Bi**, and **Ci** show each channel separately CD4 (red) ICOS (green), PD-1 (white). **Di** shows all channels together, CD4, ICOS, PD-1, and DAPI. **Aii**, **Bii**, and **Cii** show the binary layer for each channel. In **Dii** the binary layers for each channel are shown together. In **Diii** the area where CD4/PD1/ICOS intersection is shown in magenta highlighting the tight restriction of these $CD4^{pos}ICOS^{pos}PD1^{pos}$ cells to the germinal centre. Scale bars represent 50μm.

Figure S2. Phenotype of intra- and interfollicular $CD4^{pos}$ T cells in FL (**a**) Mean intensity of CD4 expression is significantly lower in the follicular $CD4^{pos}$ T-cells in FL than in interfollicular $CD4^{pos}$ T-cells (left) and the mean intensity of PD-1 in follicular $CD4^{pos}PD1^{pos}$ T-cells is significantly higher than in interfollicular $CD4^{pos}PD1^{pos}$ T-cells (right) (n= 81 follicular areas and 81 interfollicular areas from n=5 FL cases). (**b**) The intensity of expression of Bcl-6 is significantly higher in $CD3^{pos}PD\text{-}1^{pos}ICOS^{pos}$ cells than in $PD\text{-}1^{neg}ICOS^{neg}$ T-cells but is highest in FL B-cells (n=290 cells from n=15 images in n=5 FL cases). Scale bar represents 5μm. (**c**) $PD1^{pos}$ $ICOS^{pos}$ cells within the follicles are $CXCR5^{pos}$ which further confirms their identity as T_{FH} but is unhelpful in differentiating them from other follicularly located cells which all express CXCR5. (**d**) No $CD8^{pos}$ cells are found to express BCL6 confirming that CD3 is an acceptable surrogate for CD4 in these experiments.

Figure S3. Distribution and phenotype of FOXP3^{pos} cells in FL and GCs. (a1). FOXP3^{pos} cells are distributed mainly around the border of the follicle and there are also scattered FOXP3^{pos} cells in the interfollicular areas (scale bar = 200µm). **(a2)** The area in the white rectangle in a1 has been enlarged. Some FOXP3^{pos} cells express either ICOS or PD1 (scale bar = 50µm). **(b)** Binary layers of a high power (x60) image of a FL follicle are shown in each panel, **b1** some ICOS^{pos} (green) cells are FOXP3^{pos} (red)**. b2** some PD1^{pos} (blue) cells are FOXP3^{pos}, but in **b3** few FOXP3^{pos} cells are dually positive for both PD1 and ICOS. Overall, 25.0% (6.0-28.0) of ICOS^{pos} and 4.0% (1.0-8.0) PD1^{pos} T-cells expressed FOXP3, but only 5% (1.0-8.0) of dual positive ICOS^{pos} PD1^{pos} T-cells expressed FOXP3 (n= 12 images from n=3 FL samples). **(ci)** In reactive LNs, GCs FOXP3^{pos} cells are located almost exclusively outside of the GCs. **(cii)** The same image as Ci showing only the binary layer of FOXP3 (red) highlighting the exclusion of FOXP3pos cells from the GCs.

Figure S4. Ki67^{pos} cells are CD20^{pos} B-cells. Representative low power (**a**) and magnified high power (b) images of 4 colour labelling in FL showing that 96% of Ki67^{pos} cells are CD20^{pos} B-cells. CD20 (red), Ki67 (blue), PD-1 (white), CD3 (green). Scale bars, **a** = 100µm, **b** = 10µm.

Figure S5. AID positive Ki67 cells are in close contact with PD-1^{Hi} cells. (A1) Representative image showing Ki67^{pos} (green) AID^{pos} (red) cells in close contact with PD-1^{Hi} (white) cells, scale bar represents 25µm. (A**2**) Magnified area of **1** highlighting close association between AID^{pos} Ki67^{pos} cells and PD-1^{Hi} cells, scale bar represents 5µm. Images representative of n=16 images from n=6 samples. (b) Negative control demonstrating that signal seen in red channel is not autofluorescence or false positive signal from secondary antibody (negative control performed by labelling with the same secondary antibodies as in figure S5a but with no primary antibodies, counterstained with DAPI, image obtained using same laser power

settings and LUTs as S5a. (c) Representative z-stack image showing similar intra-cellular pattern of AID staining (red) in reactive GCs, and close localization of AID^{pos} $Ki67^{pos}$ cells with $PD1^{pos}$ cells in the light zone.

Figure S6. PD-L1 is not present on the $Ki67^{pos}$ cells in contact with $PD1^{Hi}$ cells. Representative low power (**a**) and high power (**b**) images of FL showing that PD-L1 (green) is not highly expressed on the $Ki67^{pos}$ cells (red) that are in contact with $PD\text{-}1^{Hi}$ cells (white). Scale bars represent 100µm (**a**) and 25 µm (**b**). (**c**) PD-L1 is mainly found outside of the follicles and is not present on $CD23^{pos}$ follicular dendritic cells (PD-L1, green. CD23, white. CD20, red). Scale bar represents 100µm.

In each case, the more frequent clones predominate in the follicular regions compared to the interfollicular areas

Figure S7. **Association between area of Ki67 and T_{FH} in reactive GCs.** r = 0.55, P = 0.019, n=17 GCs from n=4 samples

Figure S8: Proportion of $CD4^{pos}$ cells with dual expression of PD1 and ICOS by histological grade in FL. There is no significant difference in the proportion of $CD4^{pos}$ T cells that have a T_{FH} phenotype by histological grade in FL, p = 0.21.

Supplemental Figures:

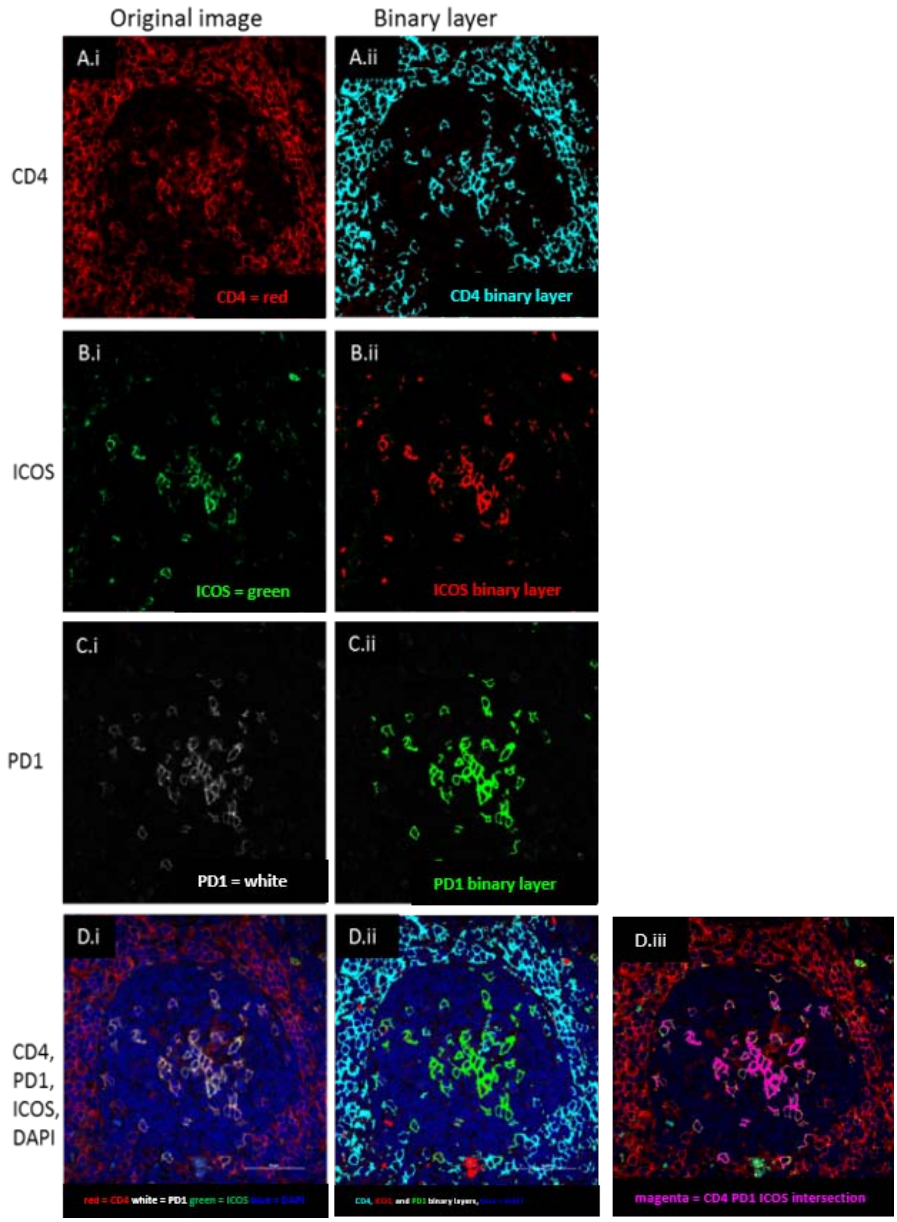

Figure S1

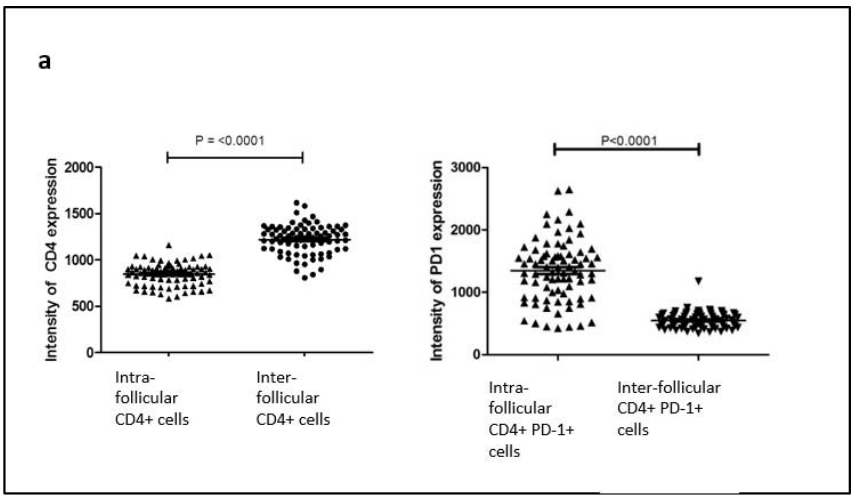
a
P = <0.0001
Intensity of CD4 expression
2000
1500
1000
500
0
Intra-follicular CD4+ cells
Inter-follicular CD4+ cells
P<0.0001
Intensity of PD1 expression
3000
2000
1000
0
Intra-follicular CD4+ PD-1+ cells
Inter-follicular CD4+ PD-1+ cells

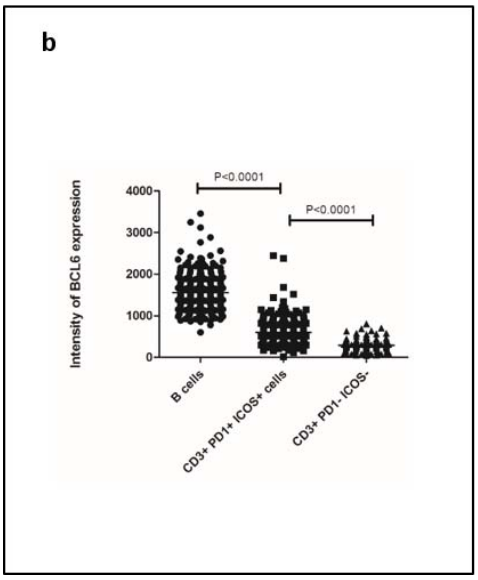
b
P<0.0001
P<0.0001
Intensity of BCL6 expression
4000
3000
2000
1000
0
B cells
CD3+ PD1+ ICOS+ cells
CD3+ PD1- ICOS-

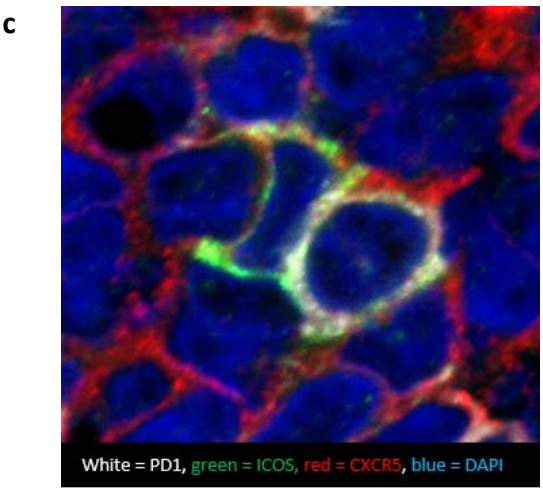
c
White = PD1, green = ICOS, red = CXCR5, blue = DAPI

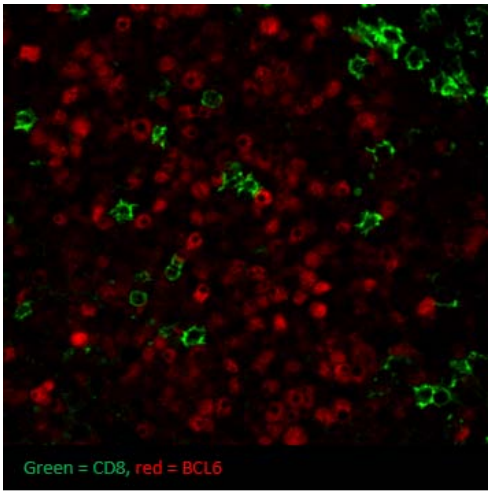
d
Green = CD8, red = BCL6

Figure S2

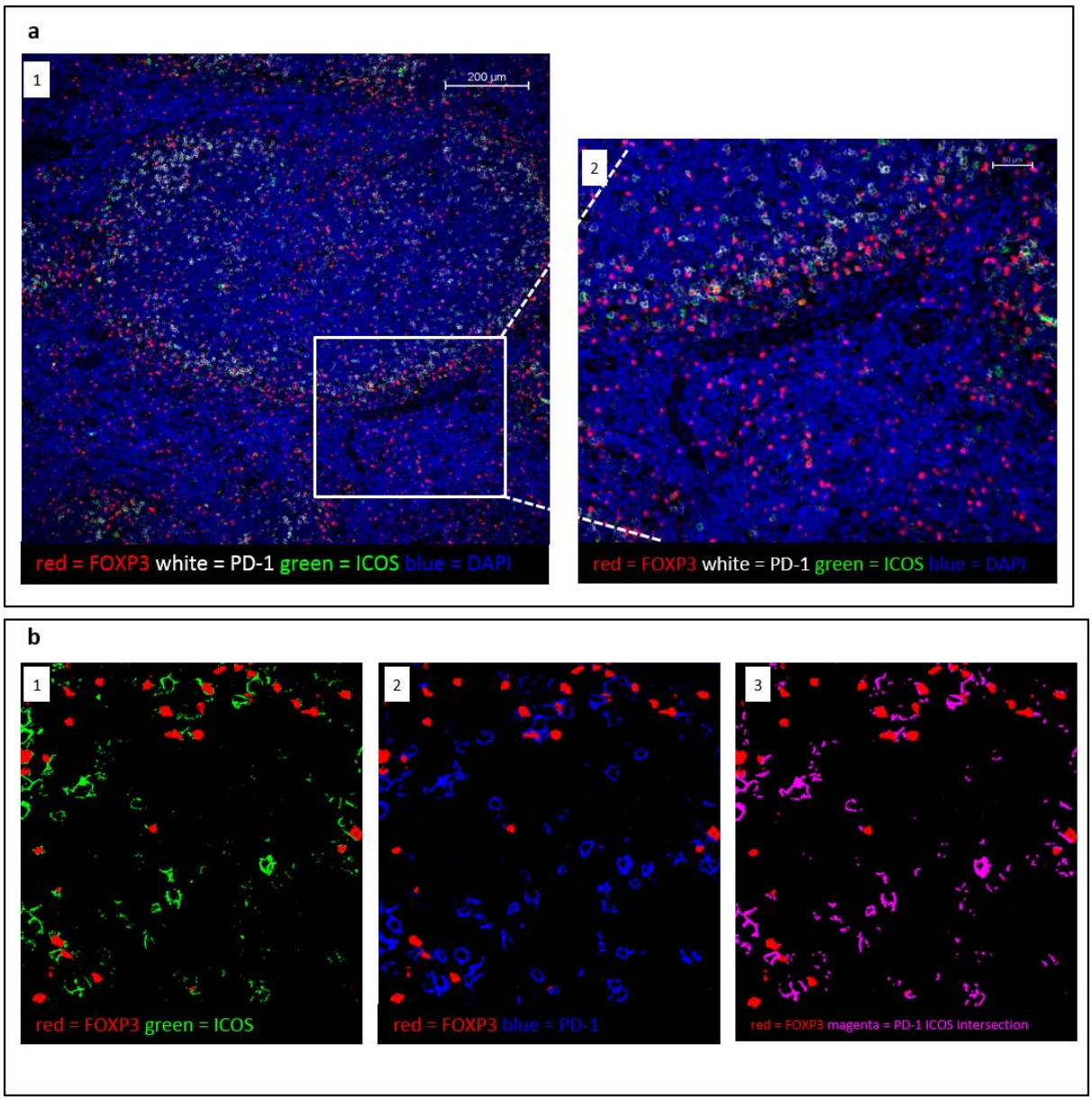
a
1
200 µm
red = FOXP3 white = PD-1 green = ICOS blue = DAPI
2
red = FOXP3 white = PD-1 green = ICOS blue = DAPI
b
1
red = FOXP3 green = ICOS
2
red = FOXP3 blue = PD-1
3
red = FOXP3 magenta = PD-1 ICOS intersection
C
1
White = PD1, green = ICOS, red = FOXP3, blue = DAPI
2
red = FOXP3

Figure S3

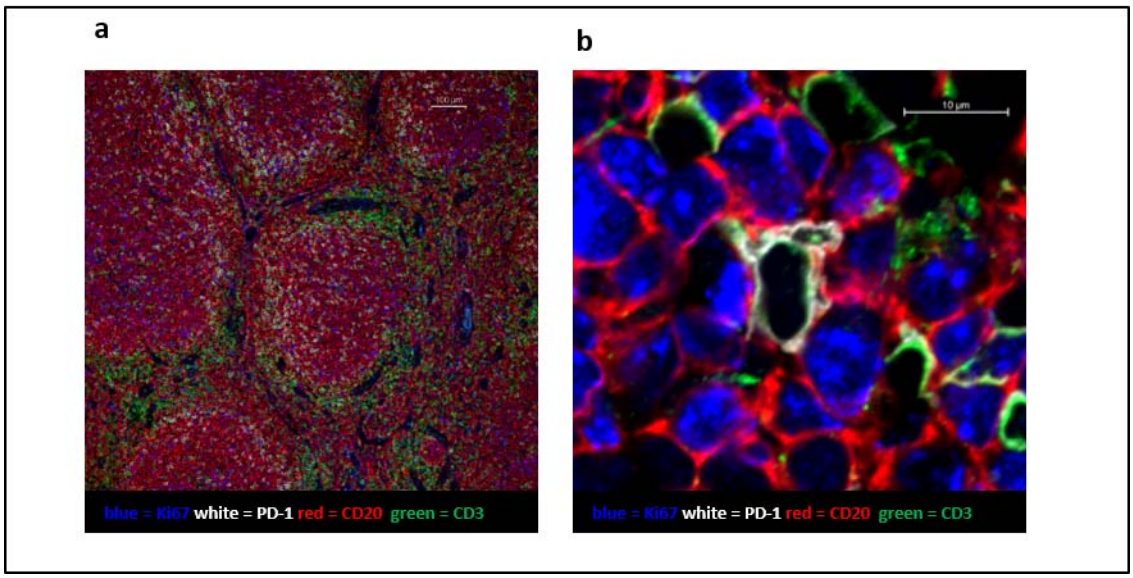
a
b
blue = Ki67 white = PD-1 red = CD20 green = CD3
blue = Ki67 white = PD-1 red = CD20 green = CD3

Figure S4

a

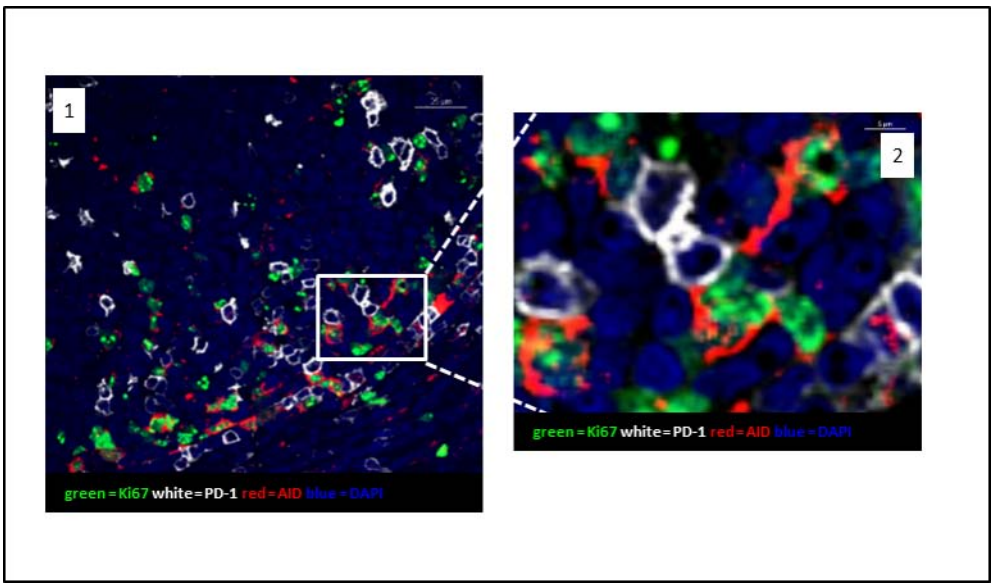

b

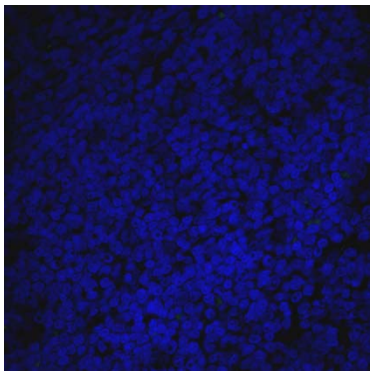

c

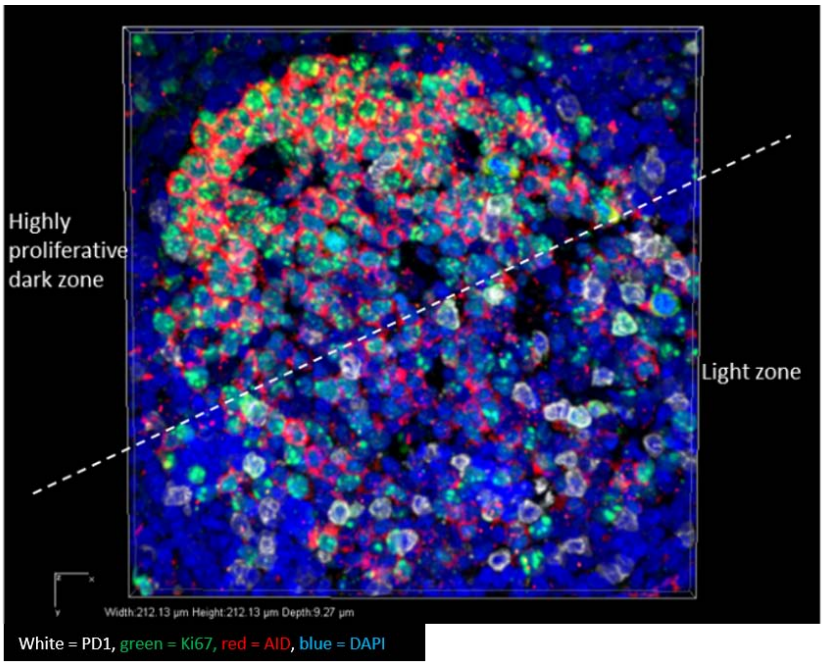

Figure S5

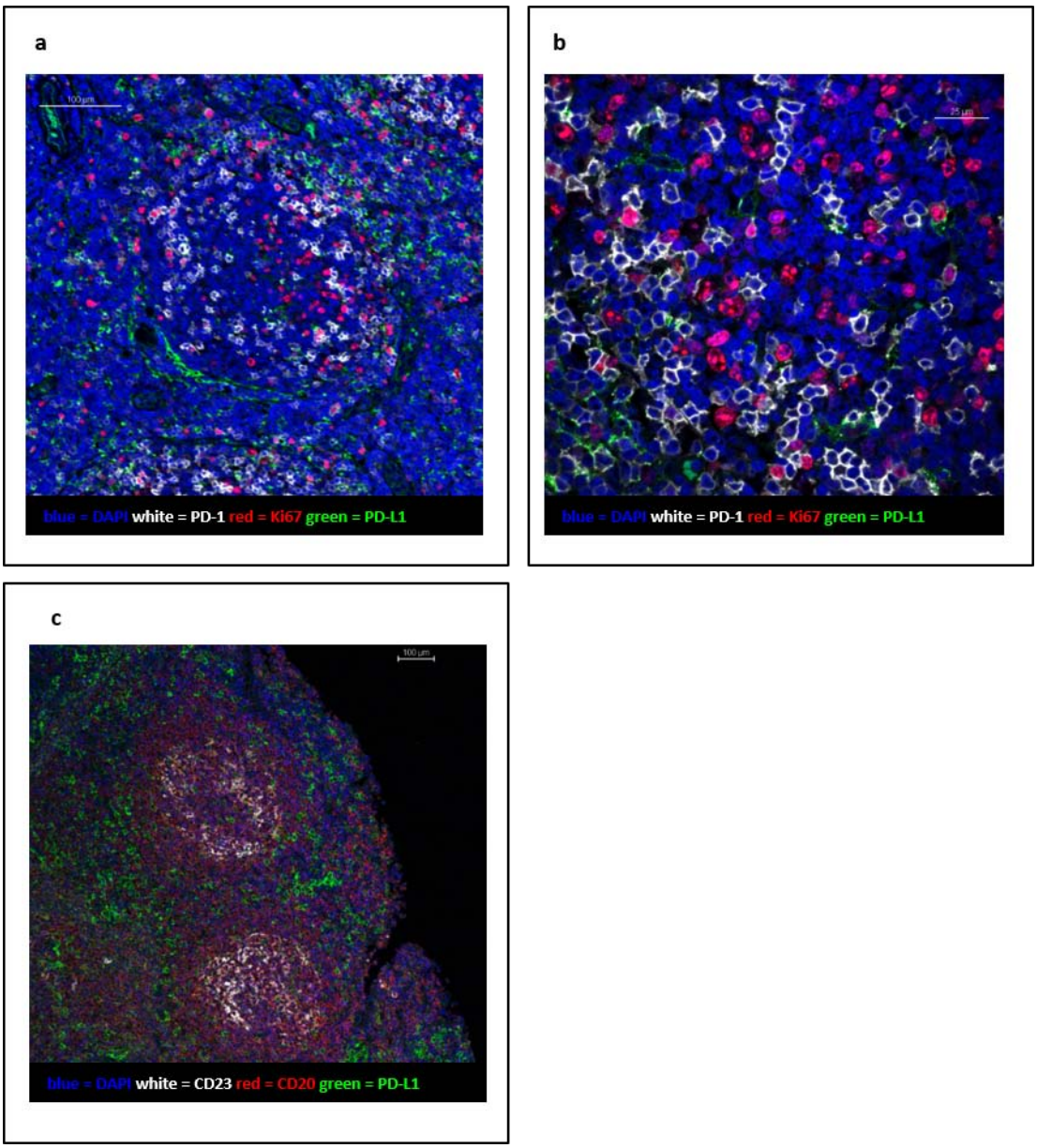
a
blue = DAPI white = PD-1 red = Ki67 green = PD-L1
b
blue = DAPI white = PD-1 red = Ki67 green = PD-L1
c
blue = DAPI white = CD23 red = CD20 green = PD-L1

Figure S6

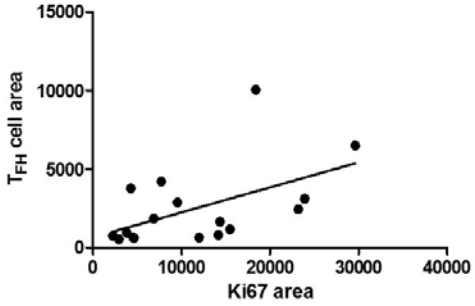

Figure S7

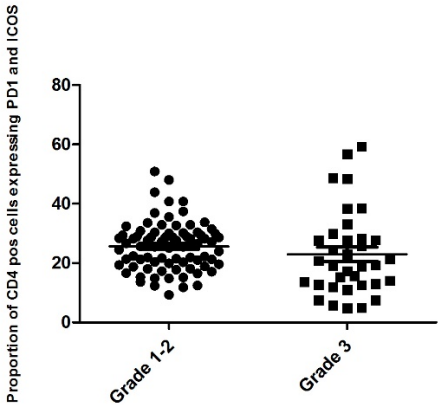

Figure S8

References

1. Sherwood AM, Emerson RO, Scherer D, et al. Tumor-infiltrating lymphocytes in colorectal tumors display a diversity of T cell receptor sequences that differ from the T cells in adjacent mucosal tissue. Cancer Immunol Immunother. 2013;62(9):1453-1461.